

Review

Advances in Metal-Organic Frameworks (MOFs) for Rechargeable Batteries and Fuel Cells

Christos Argirasis ^{1,2,*}, Niyaz Alizadeh ², Maria-Eleni Katsanou ³, Nikolaos Argirasis ² and Georgia Sourkouni ³

¹ Laboratory of Inorganic Materials Technology, School of Chemical Engineering, National Technical University of Athens, 15773 Athens, Greece

² Mat4nrg—Gesellschaft für Materialien und Energieanwendungen Mbh, Burgstätter Str. 42, 38678 Clausthal-Zellerfeld, Germany; niyaz.alizadeh@mat4nrg.de (N.A.); nikos.argirasis@mat4nrg.de (N.A.)

³ Clausthal Centre of Materials Technology (CZM), Clausthal University of Technology, 38678 Clausthal-Zellerfeld, Germany; maria.eleni.katsanou@tu-clausthal.de (M.-E.K.); cogsa@tu-clausthal.de (G.S.)

* Correspondence: amca@chemeng.ntua.gr

Abstract: The growing demand for energy, coupled with the unsustainable nature of fossil fuels due to global warming and the greenhouse effect, have led to the advancement of renewable energy production concepts. Innovations such as photovoltaics, wind energy, and infrared energy harvesters are emerging as viable solutions. The challenge lies in the stochastic nature of renewable energy sources, which necessitates the implementation of electrical energy storage solutions, whether through batteries, supercapacitors, or hydrogen production. In this regard, innovative materials are essential to address the questions associated with these technologies. Metal-organic frameworks (MOFs) are crucial for achieving clean and efficient energy conversion in fuel cells and storage in batteries and supercapacitors. Metal-organic frameworks (MOFs) can be used as electrocatalytic materials, membranes for electrolytes, and energy storage materials. They exhibit exceptional design versatility, large surface, and can be functionalized with ligands with several charges and metallic centers. This article offers an in-depth examination of materials and devices utilizing metal-organic frameworks (MOFs) for electrochemical processes concerning the generation, transformation, and storage of electrical energy. This review specifically focuses on rechargeable batteries and fuel cells that incorporate MOFs. Finally, an outlook on the potential applications of MOFs in electrochemical industries is presented.



Academic Editors: Junkai Wang, Jicheng Zhang and Qian Guo

Received: 25 March 2025

Revised: 4 May 2025

Accepted: 9 May 2025

Published: 14 May 2025

Citation: Argirasis, C.; Alizadeh, N.;

Katsanou, M.-E.; Argirasis, N.;

Sourkouni, G. Advances in

Metal-Organic Frameworks (MOFs)

for Rechargeable Batteries and Fuel

Cells. *Batteries* **2025**, *11*, 192. <https://doi.org/10.3390/batteries11050192>

Copyright: © 2025 by the authors. Licensee MDPI, Basel, Switzerland. This article is an open access article distributed under the terms and conditions of the Creative Commons Attribution (CC BY) license (<https://creativecommons.org/licenses/by/4.0/>).

1. Introduction

Projections indicate that global energy demand may reach as high as 500 EJ annually by the year 2050. The imperative for clean and alternative energy sources stands as one of the most significant challenges facing 21st-century science [1]. The worldwide trend of urban growth, along with an increasing population, have led to a marked rise in the release of greenhouse gases, particularly carbon dioxide. There exists a consensus regarding the necessity to diminish greenhouse gas emissions and to transition energy generation towards environmentally sustainable and renewable sources, such as photovoltaics and wind energy. Given that these sources do not generate a constant flow of electrical energy, it becomes essential to implement a system for storing the energy produced that is not utilized

immediately [2]. This can be achieved through the implementation of sophisticated batteries and supercapacitors. Considering the swiftly changing transportation requirements of contemporary society, lithium-sulfur batteries (LSBs) [3] are garnering interest as the next-generation power sources for diverse future aerial transportation modalities, encompassing urban air mobility and drones. This results from their competitive pricing and elevated potential energy density of 2600 Wh kg^{-1} [4]. An alternative approach involves the production and storage of hydrogen, which can subsequently be utilized in fuel cells to generate electricity and heat precisely when needed. Metal-organic frameworks (MOFs) constitute an innovative class of materials that have garnered significant attention in the last twenty years. MOF materials offer considerable benefits owing to their large specific surface area and plentiful Lewis acid sites present on their surfaces. Metal-organic frameworks (MOFs) demonstrate considerable promise in improving battery performance. Thanks to their unique structure and characteristics, MOFs significantly improve the conductivity, stability, and cycle life of batteries, presenting new possibilities for future energy storage technologies, catalytic processes, and gas separation [5–8].

Metal-organic frameworks (MOFs) are characterized by open networks created from metal-centered secondary building units (SBUs) that are interconnected by organic components. This results in the development of extensive one-dimensional (1D), two-dimensional (2D), or three-dimensional (3D) structures [9,10]. The networks show a crystalline character, indicating long-range order. Uniform pores or channels are integrated throughout the framework, often absorbing moieties such as solvents incorporated during synthesis or counter ions that neutralize the entire charges on the entire structure due to the charged metal nodes [6,8,11]. In contrast to other porous substances like zeolites and carbon-based materials, the distinguishing characteristic of metal-organic frameworks (MOFs) is their ability to achieve a “directed” architecture by the meticulous selection of both metals and organic linkers [12–14].

In addition to the conventional hydrothermal preparation method [15], various alternative techniques such as electrochemistry [15,16], sonochemistry [17,18], microwaves [19], and mechanochemistry [20,21] have been employed, frequently leading to distinct properties of the same MOF [22], for the synthesis of MOFs and their derivatives.

MOFs provide an ideal environment for electrochemical processes because of their large surface area, rendering them promising options for electrochemistry, (electro)catalysis, and energy storage applications. In comparison to other porous materials like activated carbon and zeolites, MOFs exhibit enhanced architectures and functions. However, the low conductivity (below $10^{-10} \text{ S cm}^{-1}$) of the majority of MOFs hinders their practical electrochemical applications, highlighting the need for improvement. Materials with a high density of charge carriers can serve as either metallic conductors or semiconductors [23,24]. MOF materials present considerable promises for improving electronic and proton conductivity, attributed to their functional pore surfaces, elevated surface areas, and broad structural tunability (Figure 1). A comprehensive overview of the advancements in conductive MOFs is available in [25–27]. Zhang et al. [24] provide a review of extensive improvement strategies for electronically and ionically conductive MOFs, along with recent advancements in the field.

This manuscript seeks to deliver an extensive examination of the most recent advancements in the utilization of MOFs in electrochemical devices for the purposes of electrical energy production and conversion. The analysis includes considerable challenges and constraints regarding the large-scale applications of MOFs, and potential advancements in MOF-based conductors.

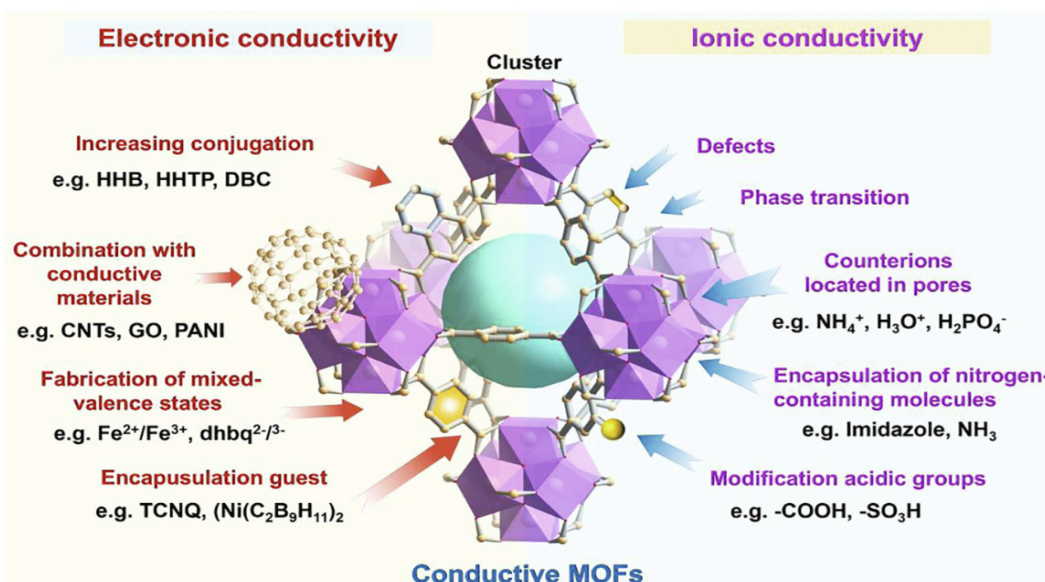


Figure 1. Schematic illustrations of the MOF materials as a versatile platform for electronic conduction and ionic conduction (Reproduced from [24] with permission).

2. Metal-Organic Frameworks (MOFs) in Batteries

The continuous rise in worldwide demand for energy has necessitated that politicians and scientists continue to pursue more efficient and environmentally friendly energy options for the future.

Batteries are essential components in the advancement of energy conversion and storage projects for the future. However, challenges persist not only in power capacity and longevity, but primarily in the scalability and environmentally sustainable production methods of battery systems.

The battery's cathode, serving as the source of the oxidizing agent, is essential to the functionality of both primary and secondary batteries. Modern cathodes require features such as structural and chemical stability, rechargeability, longevity, and safety. Researchers have extensively investigated resilient materials for electrode formation that can maintain the necessary specific capacity together with ionic and electronic conductivity during continuous cycling [28–31].

In this context, metal-organic frameworks (MOFs) have been recognized as a promising category of materials for the direct use in cathode electrodes or as precursors for the fabrication of cathode electrodes. Metal-organic frameworks (MOFs) can be manufactured by many scalable methods, from many educts [32–34] yielding nanomaterials with unique geometries and porosity that demonstrate beneficial electrochemical characteristics [35–37].

Scientists have extensively investigated resilient materials for electrodes that can maintain the necessary specific capacity and ionic and electronic conductivity, as well as catalytic activity throughout continuous cycling. In this context, metal-organic frameworks (MOFs) have been recognized as a promising category of materials for the fabrication of cathode electrodes or as precursors for cathode electrodes [38–41].

Metal-organic frameworks (MOFs) including ZIF-8 [42–46], ZIF-67 [47–49], MOF-74 [50], MOF-5 [51–53], MIL-53 [54], MIL-120 and MIL-122 [55], DUT-4, DUT-5 [55,56], and HKUST-1 [57,58], together with its derivatives, have been examined as prospective electrode materials for several battery types, including metal-ion, lithium, and metal-air batteries. The previously described battery types exhibit several distinctions in cathode activity, resulting in MOFs fulfilling different roles in each application. MOFs often offer an increased specific surface area with several mass diffusion channels for ions, enhancing the

interaction between the electrolyte [28,59,60] and the entire active surface area through their inherent micro-porosity or the engineered macro-meso-porosity among the particles [61–63]. This approach can enhance the starting capacity of the electrode and expedite the kinetics of redox reactions.

A literature survey indicates that metal-organic frameworks (MOFs) are predominantly regarded as optimal precursors or sacrificial templates for generating carbonaceous materials or oxides post-thermal treatment. Consequently, the use of pristine MOFs in batteries is restricted or entirely absent for specific battery types, including lithium-selenium [64], sodium-ion [65,66], and zinc-air [67–69]. The pyrolysis of MOFs is an efficient method for producing carbon matrices with designed molecular structures, as MOF-derived carbons retain the morphological features of the used precursor materials [38,70–72].

As a result, researchers are able to leverage the intrinsic conductivity of carbon and explore various carbon network architectures to achieve the ideal property combination for each type of battery cathode.

2.1. Lithium-Ion Batteries

Lithium-sulfur [73–75] and lithium-selenium [64] batteries are highly promising technologies, providing substantial theoretical capacity ($1\text{ C} = 1672\text{ mAh g}^{-1}$), sustainability, and low production costs [76,77].

Sulfur acts as the active element of the cathode. However, it is incapable of functioning autonomously as an electrode, requiring a supporting material for its containment.

During the discharge process, lithium ions transfer from the electrolyte to the saturated host, leading to the synthesis of lithium sulfide via several redox reactions and intermediary compounds [78]. Despite the insolubility of sulfur and its reduction products, the polysulfide intermediates exhibit significant mobility and solubility in typical electrolytes, migrating towards the anode and generating short-chained polysulfides that subsequently diffuse back. This cyclical diffusion results in anode corrosion, contributing to self-discharge and diminished cycling stability [79,80]. As a result of the shuttle effect, scientists have exerted considerable effort to create innovative cathode materials capable of effectively encapsulating sulfur and restricting its migration [81–83]. Pristine MOFs and their derived materials have been examined as sulfur hosts because of their high surface area and pore structure, particularly carbon derivatives that demonstrate enhanced electrical conductivity and structural flexibility.

The earliest publication on using MOFs in a Li-S battery was MIL-100 (Cr) by Demir-Cakan et al. [84]. It is constructed from trimesic acid linkers and chromium octahedra, including mesoporous cages measuring 25–29 Å and a pore volume of approximately $1\text{ cm}^3\text{ g}^{-1}$. Liquid sulfur (melting point is 115 °C) is introduced into the porous structure at 155 °C; a minimum of 25 wt% carbon is required for the electrode preparation to enhance conductivity. Despite the insufficient attachment of polysulfide anions to the framework and the possible hindrance of sulfur at the inner tube surfaces by the carbon matrix, the cathode capacity stayed under 500 mAh g^{-1} after 50 cycles. The vanadium modification was tested for over 200 cycles at 0.1 C, exhibiting a capacity of approximately 550 mAh g^{-1} . In contrast, a composite based on reduced graphene oxide showed slightly higher efficiency, achieving 650 mAh g^{-1} at 0.1 C after 75 cycles and 450 mAh g^{-1} for 300 cycles at 0.5 C, although these results are not directly comparable [85].

Hong et al. [86] synthesized Cu-TDPAT using the 2,4,6-tris(3,5-dicarboxylphenylamino)-1,3,5-triazine ligand in varying sizes by modifying the molecular weight. The incorporation of nitrogen-rich chemical groups from the triazine linker (basic sites) and the available metal sites of $\text{Cu}_2(\text{COO})_4$ (acidic sites) has yielded an architecture including three types of cages for sulfur containment. Type A is analogous to the HKUST-1 cage, type B employs

four ligands to form a tetrahedral cage measuring 14 Å, and type C uses eight ligands to build an octahedral structure of 20.3 Å. The capacities after 300 cycles at 0.5 C are 352, 436, 631, and 831 mAh g⁻¹ for particle sizes of 1000, 500, 200, and 100 nm, respectively.

HKUST-1 (Cu-BTC) is among the most renowned and extensively researched copper MOFs. Wang et al. [87] have reported a conventional approach of producing sulfur cathodes, which involves impregnating sulfur into the MOF pores through diffusion, to a straightforward mechanochemical mixing process. The confined environment of sulfur not only inhibits its dissolution into the electrolyte, but additionally delays its sublimation by 40 °C. The reversible interaction between sulfur and open Cu²⁺ sites enhances battery performance, attaining 500 mAh g⁻¹ after 170 cycles (at a charge/discharge rate of 0.1 C/0.05 C), compared to around 250 mAh g⁻¹ for the milled sample.

The milling procedure, now utilizing ethanol, was recently reexamined, yielding comparable findings [88]. The cell commenced with a maximum capacity of 620 mAh g⁻¹, stabilized at 280 mAh g⁻¹ after the 10th cycle, and concluded with 200 mAh g⁻¹ after 100 cycles at 0.1 C. To achieve elevated performance, additional fine tuning of sulfur and carbon black quantities is required. However, an increase in carbon black for enhanced conductivity may negatively impact sulfur loading.

Feng et al. have investigated Cu [89] and Co [90] metal centers using varying sulfur weight ratios (1:1, 1:2, and 1:3 MOF:S) according to the BTC linker. The chemical interactions between the functional groups of the MOF and sulfur have been investigated using XPS and DFT. In both MOFs, the 1:2 ratio yielded superior performance; nevertheless, the copper variant exhibited higher specific capacities (1051 mAh g⁻¹ after 300 cycles at 0.12 C) compared to the cobalt variant (600 mAh g⁻¹ after 100 cycles at 0.1 C).

The association between particle size and capacity was examined for HKUST-1, indicating a reduced capacitance for bigger particles [57]. Samples measuring 0.16, 1.6, and 5.9 mm have been prepared, resulting in capacities of 679, 540, and 480 mAh g⁻¹, with retentions of 64%, 60%, and 54%, after 20 cycles at 0.1 C. The utilization of sulfur could be enhanced due to the increased surface area and the shortened electron diffusion path for the reduction in sulfur groups within the framework. Zhou et al. [56] came to the same finding regarding the relation of particle size and reversible capacities in ZIF-8, alongside their investigation of HKUST-1, MIL-53 (Al), and NH₂-MIL-53 (Al). Particles measuring 150 nm, 1 mm, and 3 mm have been tested for 100 cycles at a rate of 0.5 C, yielding capacities of 733, 556, and 491 mAh g⁻¹, respectively. A subsequent comprehensive analysis, including sizes of 2 mm, 800 nm, 200 nm, 70 nm, and 15 nm demonstrated capacities of 489, ~570, ~765, ~860, and 968 mAh g⁻¹, with retention rates of 45%, 57%, 75%, 50%, and 22% after 250 cycles at 0.5 C [91]. In conclusion, sulfur utilization enhances with decreased particle size. However, optimal cycling stability is attained at an intermediate size.

To achieve ZIF-8 with ordered micro- and macro-porosity, the PMMA template of nanosized spheres was used for synthesizing ZnO precursor material for the fabrication of S-3DOM ZIF [92]. In comparison to the standard ZIF-8 sample, it exhibits a superior capacity of 674 mAh g⁻¹ after 500 cycles at 2 C, with a retention of 84%, as opposed to 345 mAh g⁻¹ (52.3% retention). The enhanced efficiency can be attributed to the intensified interaction between 3DOM ZIF and polysulfides, as analytically confirmed by means of UV-Vis and XPS. Liu et al. [93] have prepared a ZIF-8@RGO free-standing film via suction filtration and subsequently freeze-dried using liquid nitrogen and additional carbonization at 800 °C for 3 h, resulting in a ZIF-8@RGO scaffold rich in N/Zn active sites (Figure 2).

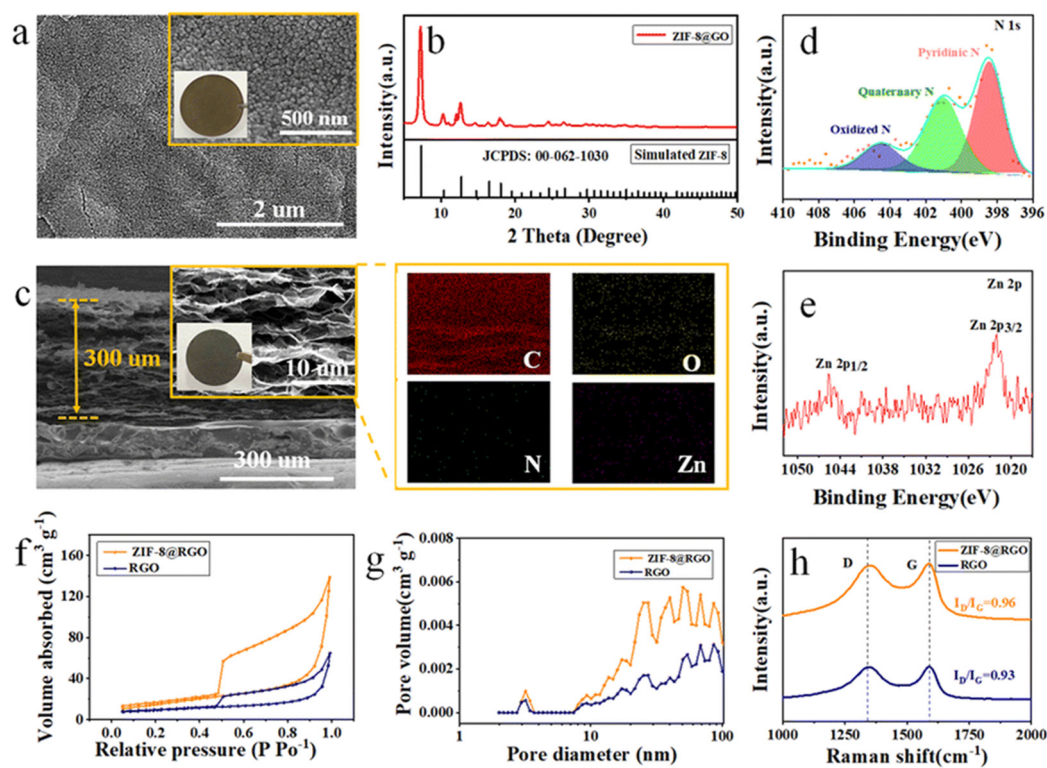


Figure 2. Characteristics of ZIF-8@RGO. (a) SEM image of pure ZIF-8; insets: enlarged microstructure and optical image of ZIF-8@RGO film. (b) XRD patterns of ZIF-8@RGO. (c) Fracture morphology of SEM and corresponding EDS mapping for C, O, N, Zn elements of ZIF-8@RGO; inset: optical picture of the free-standing ZIF-8@RGO film. High-resolution XPS spectra of (d) N 1s and (e) Zn 2p of ZIF-8@RGO. (f) Nitrogen adsorption–desorption isotherms and (g) the corresponding pore size distributions calculated from the non-local density functional theory model. (h) Raman spectra of RGO and ZIF-8@RGO (Reproduced from [93] with permission).

When compared to other metal-organic frameworks, the maximum discharge capacities observed for ZIF-8, HKUST-1, NH₂-MIL-53, and MIL-53 were 738, 431, 568, and 793 mAh g⁻¹, respectively, following 300 cycles at a rate of 0.5 C. At the end of the cycling procedure, the capacities decreased to 75%, 66%, 58%, and 44% of their maximum values, accordingly. The reduction in capacity of HKUST-1 is attributed to its significant particle size, which exceeds 10 nm [56]. Bai et al. [94] proposed a different approach to sulfur melt diffusion by generating *in situ* encapsulated S nanoparticles during the synthesis of the MOFs. A direct comparison of ZIF-8 at 800 nm, ZIF-67 at 1 μm, and HKUST-1 at 500 nm revealed suboptimal results for both initial capacities and after 1000 cycles at 0.2 C, with values of 255–170, 260–155, and 340–250 mAh g⁻¹, in each case.

Ge et al. [95] demonstrated the synthesis of ZIF-67 by incorporating tannic acid for 5 or 10 min as a modulator. It effectively shapes the structure by cleaving Co-N bonds and facilitating N-H bond formation, thereby adjusting polarity and limiting the solubility of polysulfide intermediates in the electrolyte. A further benefit is that the -OH groups of tannic acid can capture lengthy polysulfides, transforming them into insoluble polysulfide and thiosulfate; therefore, alleviating the shuttle effect [4,79]. A period of 5 min provides enhanced cycling stability over 100 cycles at a current density of 100 mA g⁻¹, yielding a capacity of 757 mAh g⁻¹ compared to 500 mAh g⁻¹ (10 min) and 422 mAh g⁻¹ (standard ZIF-67) [95]. The electrochemical efficiency of the ZIF-67-S, ZIF-67-5-S, and ZIF-67-10-S cathodes is presented in Figure 3. Also, a capacity of 521 mAh g⁻¹ during an extended cycling period (550 cycles) at a rate of 500 mA g⁻¹ is illustrated. Tannic acid has been

utilized to synthesize a hollow ZIF-8/CNT composite exhibiting commendable cycling stability [96].

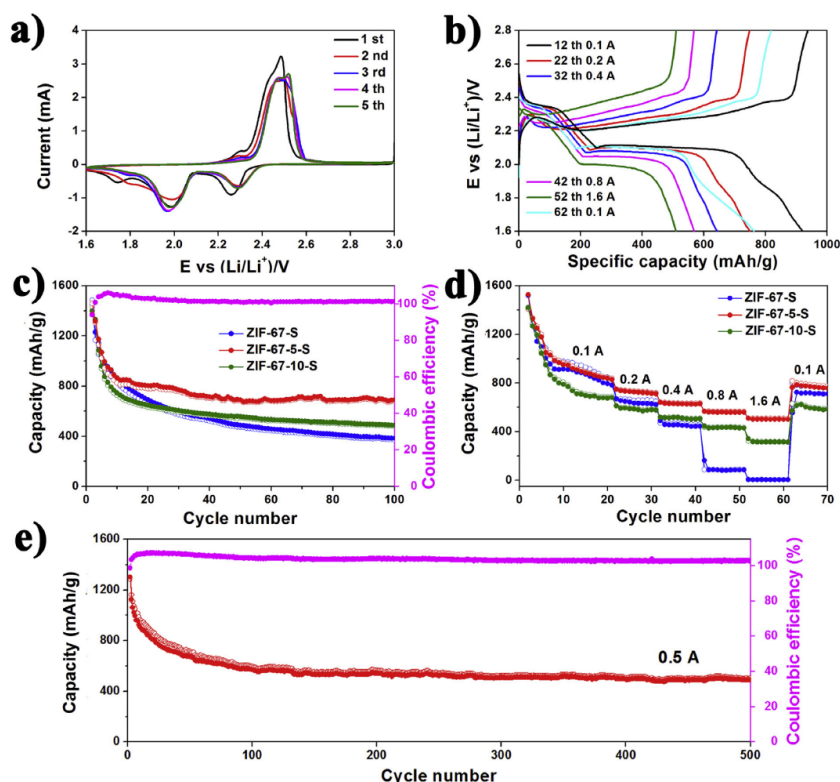


Figure 3. Electrochemical performance of ZIF-67-S, ZIF-67-5-S, and ZIF-67-10-S cathodes. (a) CV curves of ZIF-67-5-S cathode at a scan rate of 0.1 mV/s in the potential range of 1.6–3.0 V. (b) Galvanostatic charge–discharge profiles of ZIF-67-5-S cathode at various current densities in the potential range of 1.6–2.8 V. (c) Cycling performance and coulombic efficiency at a current density of 100 mA/g. (d) Rate capability for ZIF-67-S, ZIF-67-5-S, and ZIF-67-10-S. (e) Long cycle life for ZIF-67-5-S cathodes at a current density of 500 mA/g (Reproduced from [95] with permission).

MOF-5 is another viable material, having a maximal surface area of $3800\text{ m}^2\text{ g}^{-1}$ [97]. The cathode synthesized at room temperature exhibited a starting capacity of 1476 mAh g^{-1} , stabilizing at around 624 mAh g^{-1} after 10 cycles, and resulting after 200 cycles at 0.2 C to a capacity of 609 mAh g^{-1} [98]. Wang et al. [99], prepared three variants of MOF-525 (contains Zr), utilizing porphyrin linkers, and evaluated them across 200 cycles at a rate of 0.5 C. Specifically, MOF-525(Cu) attained a capacity of 704 mAh g^{-1} , while MOF-525(FeCl) and MOF-525(2H) exhibited capacities of 616 and 402 mAh g^{-1} , respectively. This arrangement is prompted by the configuration offering two, one, and zero Lewis acidic sites, respectively, capable of interacting with sulfur and polysulfides. These sites likewise provide capacities exceeding 400 mAh g^{-1} at a rate of 5 C. Liu et al. [100] have investigated 2,6-Zr-AQ-MOF and 1,4-Zr-AQ-MOF, which are zirconium metal-organic frameworks utilizing anthraquinone linkers. The high density of AQ groups inside the MOF architecture explains the improved performance of 1,4-Zr-AQ-MOF during 300 cycles at 4 C (403 vs. 300 mAh g^{-1}). The 1,4 configuration is directed into the pore, facilitating tighter contacts with neighboring AQs, while the AQs in 2,6-Zr-AQ-MOF are oriented along the framework, indicating that pore geometries play a vital role in regulating charge conduction (Figure 4). Lai et al. [101] prepared and tested cathodes for lithium-ion batteries based on MOFs with Anthraquinone-2,3-Dicarboxylate ligands.

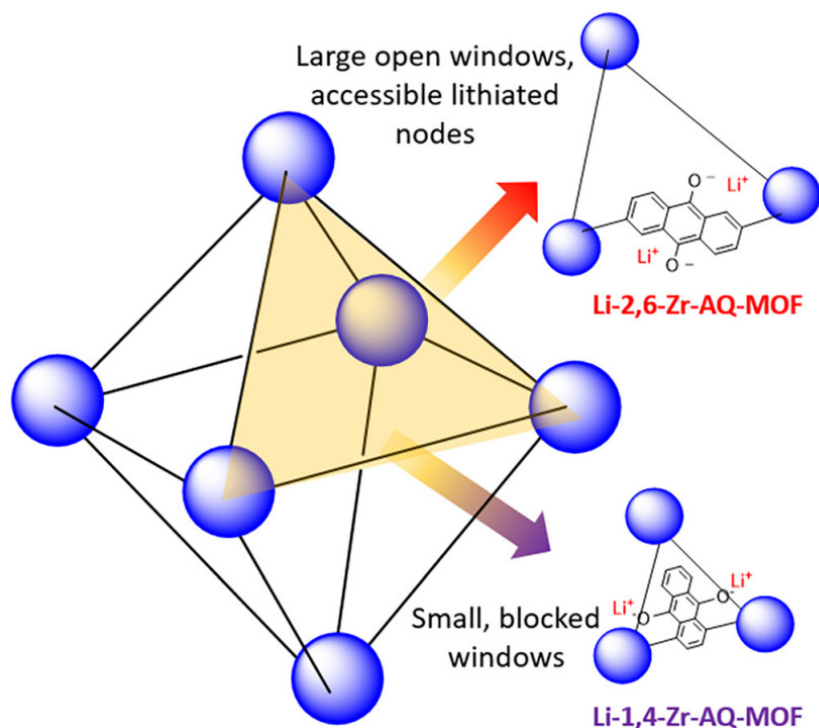


Figure 4. Ion accessibility to the Zr nodes is attenuated in Li-1,4-Zr-AQ-MOF due to smaller and more blocked pore windows compared to Li-2,6-Zr-AQ-MOF (Reproduced from [100] with permission).

Another important utilization for MOFs in Li-S batteries is in the field of separators [5]. Ngo et al. [76] have used glass fiber after modification with a bimetallic MOF as separator. This has enhanced the cycling efficiency of the new cell relative to the unmodified glass-fiber cell by a factor of two. A novel separator based on a 2D MOF/PP composite inhibited the polysulfide shuttle effect and increased the ionic conductivity leading to an enhancement of the sulfur cathode's electrochemical performance [102].

NiCo-MOF is notably intriguing as an electrode material to investigate the electrolyte/electrode interface, owing to its inherent porosity and ultrathin nanomorphology, which provide a substantial surface area that enhances the interaction between the electrode and the electrolyte. The ultrathin design reduces ion transport paths, guaranteeing that interfacial reactions prevail over bulk effects, rendering it optimal for investigating interfacial phenomena. Moreover, NiCo-MOF-derived NiCo₂O₄ exhibits mixed-valence states of Ni and Co, which augment redox processes. The redox-active sites exhibit significant sensitivity to the interface, facilitating the investigation of ion transport and reaction processes. Recently, a dominating pseudocapacitive behavior at high-rate performance was revealed, overcoming the structural degradation issues often encountered in NiCo-based devices. The electrode outperformed previous research with its 83% pseudocapacitive contribution, demonstrating high-rate performance and quick, diffusion-independent charge storage [103].

Utilizing both theoretical and experimental approaches, deviations in conduction processes occurred between Ni-MOF and NiCo-MOF, along with their electrochemical performance as anode materials in rechargeable lithium-ion batteries. The average conductivity of NiCo-MOF has been determined at 0.058 mS cm^{-1} , demonstrating a significant increase, being 34 times higher than that of Ni-MOF ($0.0017 \text{ mS cm}^{-1}$). Calculations using the density functional theory (DFT) suggest that the rise in conductivity results from the incorporation of Co²⁺, which enhances the electron transport pathways and markedly elevates carrier concentration. In contrast to Ni-MOF, NiCo-MOF exhibits an increase of 19 additional electrons at the Fermi level. The improved conductivity leads to a notable

enhancement in electrochemical performance; under 2 C conditions, NiCo-MOF exhibits a specific capacity of 696.3 mAh g^{-1} after 200 cycles, which is double that of Ni-MOF (299.9 mAh g^{-1}) [104].

Wei and Qin [105] proved with the example of a 2D Iron-Quinoid MOF that it is possible to macroscopically tune conductivity properties from an electronic structure using DFT calculations. The results from the DFT calculations indicated a narrow bandgap, while subsequent quantum chemical modeling of the bimetal unit within the Iron-Quinoid MOF indicated an increase in the bandgap upon gradual oxidation of the MOF structure.

Computational quantum mechanical methods typically yield detailed electronic structure information with adequate precision, offering valuable insights into the conductive behavior of MOFs. A novel design approach involves leveraging machine learning to enhance the efficiency of screening and discovering new conductive materials. Zanca et al. [106] provided a comprehensive overview of the prevalent quantum mechanical techniques utilized to characterize key band structure parameters of MOFs.

2.2. Zinc (Zn)-(Metal-Ion) Air Batteries

Metal-ion batteries, particularly lithium-ion batteries, have emerged as the most prevalent type, mostly due to their outstanding efficiency and energy density in electronic applications. Notwithstanding the prevalent application in commercial contexts, opportunities for enhancement persist by substituting transition metal oxide cathodes, such as LiMO_2 , LiM_2O_4 , and LiMPO_4 (M:Mn, Co, Ni, etc.) such as LiCoO_2 , LiMn_2O_4 , and LiFePO_4 , with metal-organic frameworks and carbon/oxide-based materials. In this respect, a composite of Mn-based MOFs and carbon nanotubes (Mn-MOF/CNTs) was synthesized for zinc-ion batteries (ZIBs) cathodes. The constructed Mn-MOF/CNT//Zn battery demonstrates a notable specific capacity of 260 mAh g^{-1} at a current density of 50 mA g^{-1} , along with impressive capacity retention of around 100% after 900 cycles at 1000 mA g^{-1} [107].

The notable electrochemical efficiency can be linked to the elevated porosity and conductivity of Mn-MOF/CNT, along with the presence of the Mn^{2+} electrolyte additive. The extensive variety of pore and morphological characteristics, along with the capacity for storage of metallic ions, renders them excellent cathode materials.

The application of MOF-177 ($\text{Zn}_4\text{O}(1,3,5\text{-benzene-tribenzoate})_2$) in lithium-ion batteries (LIBs) began almost 20 years ago with its utilization in the anode compartment [108]. Despite the results being unimpressive due to restricted cycle stability, this first assessment prompted further exploration of additional MOFs. Subsequently, the MIL group [6] was investigated as cathodes, commencing with the examination of Fe^{2+} and Fe^{3+} active sites as redox centers in MIL-53 [109] and MIL-68 [110]. MIL-53 may provide ca. 70 mAh g^{-1} by accommodating 0.6 Li/Fe, while MIL-68 can retain 0.35 Li inside its architecture. Although either MOFs utilize terephthalic acid, the divergent reaction conditions result in dissimilar pore geometries, triangular in MIL-53 [54] and hexagonal in MIL-68, elucidating the challenges associated with lithium electrolyte diffusion into the MOF structure. Formulated using the identical linker, MIL-101 was evaluated, yielding unsatisfactory findings attributed to the stability of the oxidized form (Fe^{3+}) of Fe^{2+} , resulting in capacity decline and rapid electrode deterioration [111]. The metal-organic framework (MOF) was subsequently reevaluated, demonstrating a discharge capacity of 72 mAh g^{-1} over 100 cycles at a rate of 0.2 C and an absorption of 0.62 Li/Fe [63].

Recently, Deng et al. [112] published results on the development of non-noble metal FeNi@NC-900 bifunctional air-cathode catalysts for both the oxygen reduction reaction (ORR) and the oxygen evolution reaction (OER), which represent a crucial advancement in the development of practical rechargeable zinc-air batteries (ZABs). Another iron metal-organic framework, utilizing ferrocenedicarboxylate ($\text{Fe}_2(\text{DFc})_3$), was synthesized, exhibit-

ing a remarkable starting specific capacity of 172 mAh g^{-1} at 50 mA g^{-1} and exceptional stability, maintaining ca. 70 mAh g^{-1} at 2000 mA g^{-1} for 10,000 cycles [113]. Various materials for cathodes can be employed directly in aqueous ZN-Ni batteries by doping Ni-MOF-74 with M^{x+} ions (Mn^{2+} , Co^{2+} , Cu^{2+} , Zn^{2+} , Al^{3+} , Fe^{3+}) to preserve the genuine architecture while modifying the quantity and type of metal ions [114]. Ni/Co bimetallic metal-organic frameworks (NCBMs) are excellent candidates for alkaline zinc batteries due to their exceptional physical and chemical characteristics. An alkaline zinc battery, utilizing MBene-NCBM as the cathode and zinc foam as the anode, has demonstrated a remarkable energy density of 280 Wh kg^{-1} alongside a power density of 3306 W kg^{-1} . The cycling tests reveal that the device's capacitance sustained a level of 79% following 1500 cycles [115].

Although less prevalent than iron-based MOFs, there have been several initiatives involving copper for lithium-ion batteries. Peng et al. [116] employed Cu-TCA to harness redox activity from Cu/Cu^{2+} centers and the tricarboxytriphenyl amine organic linker (N/N^+). By cycling at 0.5 C , significant capacity degradation occurred (starting at 102 mAh g^{-1} with around 39% retention after 200 cycles), likely due to the loss of redox activity of Cu ions. In contrast, at elevated C-rates ($1 \text{ C}/2 \text{ C}$), retention rates improved markedly (approximately 71%) as the electrolyte addition (hexamethylene diisocyanate) enhanced system stability and augmented discharge capacity at 2 C by 11 mAh g^{-1} . Nagatomi et al. [117] utilized a phthalocyanine linker including copper and copper ions as the metal center to construct the 2D Cu-CuPC. The integration of micropores (1.4 nm) and mesopores (11 nm) alongside the framework's moderate electrical conductivity resulted in a capacity of 52 mAh g^{-1} after 200 cycles at 0.4 C . Gu et al. [118] have reported encouraging findings with $\text{Cu}_3(\text{HHTP})_2$ (HHTP = 2,3,6,7,10,11-hexahydroxytriphenylene). The reversible capacity of 95 mAh g^{-1} from the 20th to the 60th cycle (with an 8% degradation by the end of 100 cycles) may indicate an intercalation ratio (Li:Cu) approaching 100%, linked to the layered MOF structure and its inherent conductivity.

In situ transmission electron microscopy (TEM) serves as an effective method for examining the structure and changes in composition at the atomic level during electrochemical reactions, offering a comprehensive understanding of structural degradation. During charge–discharge, virtually all metal oxides (MOs) face structural disintegration and phase separation, in contrast to graphite. The nanoscale morphological modifications that occur during charge–discharge have been investigated using transmission electron microscopy (TEM). Ordered mesoporous nickel oxide (OMNiO) was prepared and employed as the model MO. A connection between TEM and electrochemical investigations to elucidate the underlying cause of the rapid capacity decline that is prevalent in MOs in general and NiO in particular was established [119]. A comprehensive review by Xia et al. [120] examines advancements in the in situ transmission electron microscopy (TEM), emphasizing its contribution to understanding the degradation mechanisms of MOF structures in interfaces between electrodes and electrolyte, electrode surfaces, particle interior, and thermal effects. The insights obtained from in situ TEM, which is rapidly advancing, are unique and anticipated to inform the design of improved layered cathode materials.

Tian et al. [121] have created isostructural MOFs with one-dimensional and two-dimensional configurations utilizing Cd or Co as metallic centers and naphthalenediimide ligands. The two-dimensional MOFs include quadratic cavities around $20 \times 20 \text{ \AA}$ resulting in superior diffusion coefficients compared to the one-dimensional variants, attributable to their greater porosity. Despite the Co version demonstrating superior initial specific capacity, the MOF displayed instability and inadequate cycle performance. Conversely, Cd exhibited satisfactory performance with 47 mAh g^{-1} over 50 cycles at a current density of 100 mA g^{-1} .

Finally, *in situ* synthesis of MOF-74 with a sophisticated surface modification led recently to higher stability of Zn-ion battery anodes [122]. An intriguing method involves the application of MOFs on catalyst surfaces, for example, by utilizing Mn-MOF-74 to modify the surface of the Li-rich layered $\text{Li}(\text{Li}_{0.17}\text{Ni}_{0.20}\text{Co}_{0.05}\text{Mn}_{0.58})\text{O}_2$ with a 2–3 nm thick layer [123]. This approach enhances oxygen storage capacity and increases the number of surface-active sites, and at the same time, increases ion diffusion through the structure channels. Specifically, after 100 cycles, the modified composite provided a capacity of 284 mAh g^{-1} as compared to 236 mAh g^{-1} at 0.1 C, with a capacity retention of approximately 87% and overall enhanced efficiency for all C-rates up to 5 C.

2.3. Zinc (Zn)-Air (Metal-Air) Batteries

Metal-air batteries (MABs) have drawn significant interest because of their comparatively high energy density and eco-friendliness relative to other battery technologies. Zinc and lithium electrodes represent the most appealing possibilities for metal anodes [124–126]. However, their cathodes are more intricate components that permit the ingress of ambient oxygen into the system. The entire efficiency of the cell is significantly contingent upon the kinetics of oxygen electrochemistry, specifically, the OER (oxygen evolution reaction) taking place at the cathode during charging, and during discharging the corresponding oxygen reduction reaction (ORR). The primary problem concerning MABs is the creation of suitable non-noble catalysts that promote both ORR and OER while preventing premature corrosion under cycling conditions [127].

Recently, many alternatives to non-precious electrocatalysts have been investigated, including single atom catalysts [128], carbon-based materials, transition metal oxides, metal alloys, and sulfides. The inherent characteristics of these electrocatalysts, determined by the compound, are complemented by parameters such as crystalline structure, morphological characteristics, and heterostructure interfaces. These elements can greatly impact the efficiency of an electrocatalyst by improving molar diffusion pathways and increasing the availability of active sites. Metal-organic frameworks (MOFs) demonstrate structural flexibility, uniform porosity, and high surface area, indicating considerable potential for application as electrocatalytic components in MAB cathodes.

Preliminary findings on MOFs in Li-O₂ batteries were disclosed in 2014, encompassing MOF-5, HKUST-1, and MOF-74 (Co, Mg, and Mn) [51]. MOF-5 and HKUST-1 exhibited primary capacities of 1780 and 4170 mAh g⁻¹, respectively, at a current density of 50 mA g⁻¹. The open metal sites of MOF-74 confer advantages resulting in capacities of 3630 mAh g⁻¹ for cobalt, 4560 mAh g⁻¹ for magnesium, and 9420 mAh g⁻¹ for Mn, with manganese-based catalysts demonstrating exceptional performance in electrochemical applications [129,130]. However, after six consecutive cycles at 200 mA g⁻¹, a capacity decline is revealed from around 5600 mAh g⁻¹ in the first cycle to 1300 mAh g⁻¹ in the last one, which is a common occurrence as demonstrated in subsequent reports. Yan et al. [131] examined the influence of Co-MOF-74 particle size. The rod dimensions (length × breadth) were altered by choosing various ratios of DMF:H₂O, specifically 1:4 (9.5 μm × 1400 nm), 1:1 (6.5 μm × 800 nm), and 4:1 (about 240 × 20 nm). The rod structure was maintained by using salicylic acid as a regulator, which can compete with the ligand, and therefore hinder the coordination bond between metal centers and organic linkers, which affects crystal growth and size.

Lv et al. [132] reported the synthesis of “MOF-plus-MOF” single atom catalysts for Zn-air batteries. They prepared cobalt atoms stabilized by N-doped carbon using a pyrolysis step, exhibiting 3D interconnected structures, a large specific surface area, and abundant N-active species. The Co-N₃C₁ single-atom configuration contributes to the exceptional ORR/OER performance of CoSAs@NC-920, surpassing that of commercial noble metal

catalysts. Furthermore, it exhibited a greater specific capacity, enhanced discharge power density, and remarkable cycling stability than actual rechargeable zinc-air batteries.

Salicylic acid interacts analogously with 2,5-dihydroxy terephthalic acid and hence, terminating the directed chain formation and maintaining the crystal size by varying the modifier concentration. The small particles of 20 nm resulted in initial cycle capacities of $11,350 \text{ mAh g}^{-1}$ at 100 mA g^{-1} and 6440 mAh g^{-1} at 500 mA g^{-1} , significantly surpassing the capacities of 800 nm (4880 mAh g^{-1}) and 1400 nm (4710 mAh g^{-1}) at 100 mA g^{-1} . A subsequent endeavor to synthesize MOF-74 involved the creation of a bimetallic MnCo catalyst in a 1:4 ratio [133]. In contrast to mono-metallic MOFs, the synergistic effect enhances efficiency and reversibility, exhibiting an initial capacity of $11,150 \text{ mAh g}^{-1}$ at 200 mA g^{-1} and stability over 44 cycles at a threshold of 1000 mAh g^{-1} , while other samples demonstrate lower capacities of 7767 mAh g^{-1} (Mn and Co simple mixture), 6040 mAh g^{-1} (Mn-MOF-74), and 5630 mAh g^{-1} (Co-MOF-74). Nickel has also been investigated in an architecture comprising bipyridine and trimesic acid [134]. Following six cycles at 0.36 mA cm^{-2} , the capacity declines to approximately 1200 mAh g^{-1} , reflecting an 80% reduction from the initial cycle, but with a constant capacity of 600 mAh g^{-1} , it can work for 170 cycles at 0.6 mA cm^{-2} .

2.4. Metal-Organic Framework (MOF)-Based Composite Materials

2.4.1. Metal-Air Batteries (MABs)

As previously indicated, MOFs can exhibit adjustable particle sizes and hollow structures, which are maintained following their processing to generate carbon-based materials or their nanocomposites. These materials exhibit mixed ionic/electronic conductivity, making them exemplary materials for possible application in battery cathodes. Furthermore, the complete availability of their active sites is an essential characteristic for their application in MABs; thus, various MOF-derived components have been employed in gas-diffusion electrodes, mainly in zinc-air batteries (ZABs).

Numerous studies confirm that exclusive heteroatom doping of MOF-derived three-dimensional carbonaceous materials can enhance the oxygen reduction reaction (ORR) and demonstrate favorable outcomes in primary alkaline zinc-air batteries (ZABs) [61,135,136]. NaCl has been utilized as a confining agent for ZIF-8 to maintain a consistent polyhedral structure post-carbonization. The produced catalysts demonstrated commendably stable performance when used in zinc-air battery systems at laboratory scale [61,135]. Yang et al. [136] introduced a silica-assisted template technique to enhance the accessibility of graphitic N-containing sites in a ZIF-8-based catalyst, attaining an exceptional specific surface area of $254 \text{ m}^2 \text{ g}^{-1}$ via a synergistic structure comprising a macroporous structure and micromesoporous “walls”. The engineered material exhibited an exceptional specific capacity of 770 mAh g^{-1} Zn at a challenging current density of 120 mA cm^{-2} and a maximum power density of 197 mW cm^{-2} . In addition to heteroatom doping, the incorporation of metals such as Fe and Co presents a compelling approach for defining active regions within carbon matrices. The thermal treatment of MOFs often results in doping with metals or the uniform decorating of carbon-based materials with heteroatoms as well as metal atoms. ZIF-8 has been widely utilized for synthesizing Fe-N-C electrocatalysts with a certain pore hierarchy for the oxygen reduction reaction (ORR). Xu et al. [42] synthesized an Fe-N-C catalyst via the straightforward pyrolytic treatment of Fe-ZIF, achieving commendable ORR metrics ($E_{1/2} = 0.881$) and effectively utilizing it in a ZAB. They demonstrated that Fe doping not only improves the electronic conductivity of carbon structures, but also enhances the wettability of the electrocatalyst with water, a trait that may facilitate the ORR by augmenting surface exposure to the electrolyte. Ferrocene ($\text{Fe}(\text{C}_5\text{H}_5)_2$) [137] and iron carbonyl ($\text{Fe}(\text{CO})_5$) [138] have been utilized as starting materials to modify ZIF-8,

resulting in the formation of carbon compounds containing iron moieties. In all studies, the three-dimensional porous Fe-N-C electrocatalytic materials, utilized as cathode materials in zinc-air batteries, achieved steady voltage during discharge and exhibited significantly high peak power densities ($>200 \text{ mW cm}^{-2}$), surpassing Pt-decorated carbon cathodes. Under specific conditions, ZIF-8 serves as a suitable and economical precursor for the synthesis of Fe-N-doped carbon nanotubes, which have remarkable ORR catalytic activity making them attractive as catalytic materials for ZABs [139,140].

Similar treatment approaches for ZIF-8 have been utilized to synthesize Fe-N-doped C-catalysts, which can improve OER kinetics, and are therefore appropriate for use in rechargeable liquid ZABs [141,142]. Specifically, Chen et al. [141] constructed a catalytic material featuring a dodecahedral structure and refined pore distribution, resulting in an extensive surface area and facilitating exceptional ORR performance. The ZAB system not only provides a high specific capacity of 801 mAh g^{-1} and a peak power density of 184 mW cm^{-2} , but also withstands 600 continuous galvanostatic cycles of 10 min each at a current density of 10 mA cm^{-2} .

Recently, co-doped MOF-derived catalysts demonstrated significant efficacy in the oxygen reduction reaction (ORR) and oxygen evolution reaction (OER), thereby enhancing rechargeable zinc-air batteries (ZABs). They can be produced by direct pyrolysis of cobalt-containing metal-organic frameworks (MOFs), such as ZIF-67, in an inert environment [47,143]. ZIF-8 was pyrolyzed into a nitrogen-doped carbon structure (N/C) and subsequently reacted with a Co solution to produce a catalyst working effectively in both aqueous as well as solid-state zinc-air batteries [144]. The resulted catalyst demonstrated remarkable ORR and OER electrochemical characteristics ($\Delta E_{(\text{OER-OER})} = 0.65 \text{ V}$) and are extraordinarily stable, sustaining prolonged cycles of two hours per cycle at 50 mA cm^{-2} . Similarly, other morphologies of Co-NeC generated from MOFs, such as nanorods [145], nanoflake arrays [146], and hexagonal structures [147], have been investigated. Zhang et al. [147] examined the influence of MOF precursors and pyrolysis conditions using the BTC, revealing that a Co-NeC catalyst, termed Co-BTC-bipy-700, demonstrated exceptional electrocatalytic properties when employed in ZABs.

The synergetic interaction of Fe and Co atoms inside N-doped carbon-based nanostructures effectively enhances the electrocatalytic ORR and OER efficiency of the MOF derivative material. Zhong et al. [148,149] pyrolyzed FeCo@ZIF to produce dual-doped carbon polyhedral (Figure 5), which demonstrated superior ORR activity relative to single atom-doped ZIF-derived catalysts, as indicated by DFT calculations and electrochemical ORR assessments (Figure 6) [148]. Duan et al. [149] conducted a comparable DFT analysis, revealing that the FeCo-N-C catalyst exhibited bifunctional electro-catalytic capabilities, substantiated by its outstanding performance as an air electrode in a rechargeable zinc-air battery. The cathode achieved a maximum power density of 150 mW cm^{-2} and withstood 360 cycles of 15 min at a current density of 1 mA cm^{-2} .

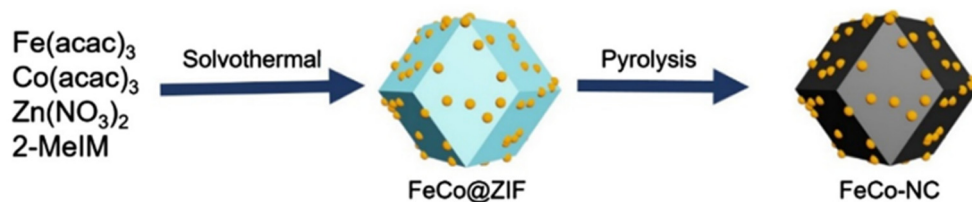


Figure 5. Schematic illustration of the synthetic process of FeCo-NC (Reproduced from [148] with permission).

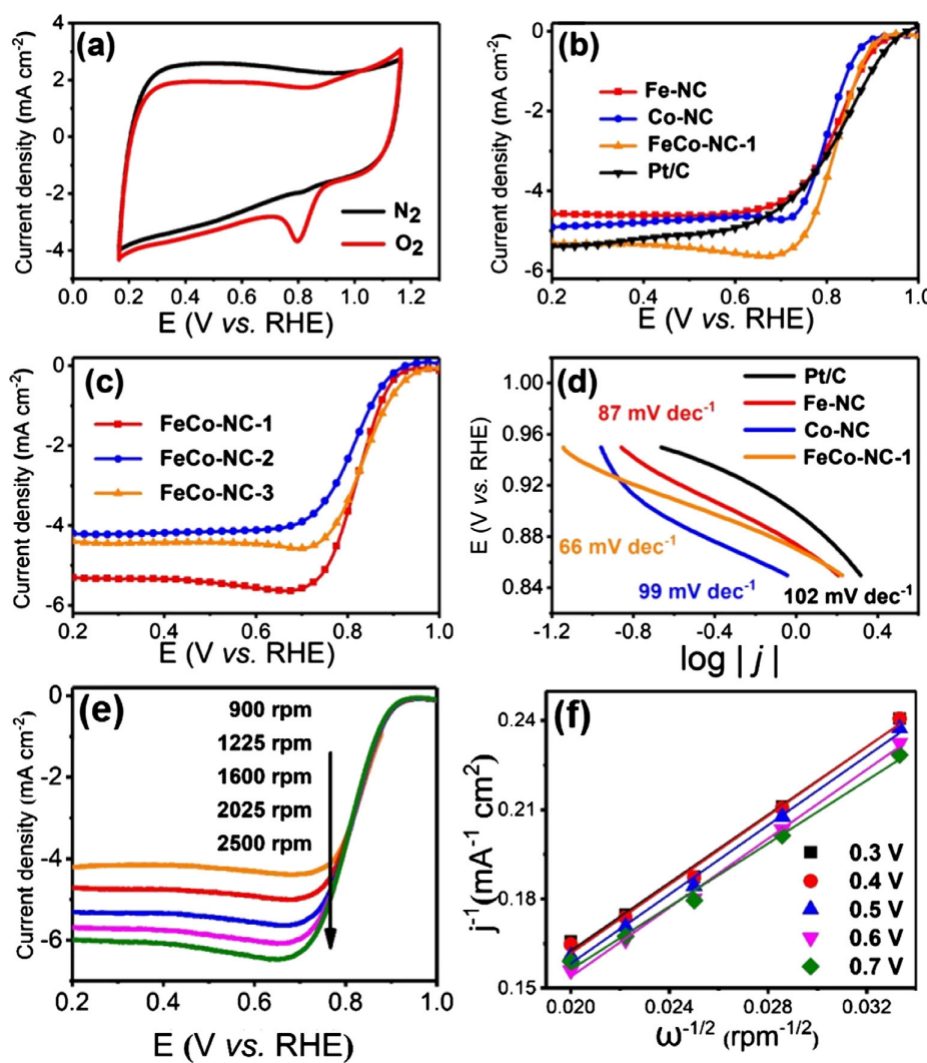


Figure 6. Electrocatalytic ORR performance. (a) CVs of FeCo-NC-1 catalyst in O_2 -saturated and N_2 -saturated 0.1 M KOH solution. (b) LSV curves of Fe-NC, Co-NC, and Pt/C. (c) LSV curves of FeCo-NC with different metal ratios. (d) Tafel plots of Fe-NC, Co-NC, FeCo-NC-1, and Pt/C. (e) LSV curves at different rotation rates and (f) K-L plots of FeCo-NC-1 (Reproduced from [148] with permission).

Carbon compounds generated from MOFs have been investigated as prospective cathodes for MABs using a lithium anode. MOF-5 has been chemically etched and pyrolyzed to eliminate the Zn-containing structure, resulting in a material with BET surface area of $1255 \text{ m}^2 \text{ g}^{-1}$, which demonstrated an initial capacity of 1437 mAh g^{-1} [150]. Ge et al. [151] introduced a templated approach for the synthesis of carbon-based cathode materials produced from ZIF-8. Polystyrene beads served as a self-sacrificial template to create macropores in addition to the micropores of the ZIF-nanomaterial, significantly enhancing the specific capacity of the cathode (5082 mAh g^{-1}).

Yu et al. [152] synthesized a molybdenum-based metal-organic framework (MOF) that, upon thermal treatment in an argon environment, yielded nitrogen-doped porous molybdenum carbide (MoC_{1-x}) characterized by extensive meso- and macroporous channels, which created active sites conducive to oxygen reactions. The constructed battery exhibited a complete discharge capacity of $20,212 \text{ mAh g}^{-1}$ at a stable voltage of 2.62 V under a current of 200 mA g^{-1} , while it yielded 1000 mAh g^{-1} over 100 cycles.

In addition to carbonaceous cathode materials, S-containing compounds obtained from Ni-MOF [153] and ZnCo-MOF [154] through hydrothermal sulphuration methods

demonstrated potential efficacy as cathodes in rechargeable Li-O₂ batteries. Ni₃Se₂ and ZnCo₂S₄ exhibit distinctive layered architectures, contributing to the MAB longer cycle life of 120 cycles at 300 mA g⁻¹ and 90 cycles at 100 mA g⁻¹, respectively.

2.4.2. Lithium Batteries

Regarding carbon MOF-derived materials, it is evident that, in addition to the feasible doping of carbon matrices, the diverse pore sizes and structures of MOF-derived carbons have the potential to directly encapsulate molecules within the pores. A significant aspect is the formulation of active electrode materials for Li-ion batteries, which can be customized to include various metals, oxides, or chalcogenides. These features satisfy the criteria for an optimally conductive carbon matrix to confine sulfur, facilitating the formation of cathodes for lithium-sulfur batteries [155].

The extensive study of ZIF-8 as a metal-organic framework precursor for lithium-sulfur materials, and examination of many distinctive nanoparticle structures of the resultant carbon, including regular rhombic dodecahedrons [156,157], spheres [158], and nanosheets [159] are reported. Nitrogen-doped two-dimensional C-nanosheets with hierarchical porosity demonstrated effective conductivity as hosts for the immobilization of sulfur. The synthesized lithium-sulfur battery exhibited a starting capacity of 1226 mAh g⁻¹ and underwent comprehensive testing at different discharge rates. Furthermore, the air electrode demonstrated the ability to withstand 300 cycles, with a retention of 65.2% at 0.2 C after 100 cycles [159]. Hao et al. [160] synthesized two-dimensional graphene-like carbon architectures via thermal exfoliation of Cu containing 4,40-bipyridine MOFs, emphasizing the hydrophilicity of the 2D-sheet walls. The results of water vapor adsorption validate the favorable surface polarity of the carbon matrix, which attracts polysulfides and improves the kinetics of redox chemistry. The constructed Li-S battery retained 99% of its capacity for 250 cycles at 0.5 C.

Kim et al. [161] introduced dual heteroatom doping of mesoporous hexagonal rod-shaped carbon nanoparticles derived from S-modified MOF-74, demonstrating that this approach enhances the capacity retention of Li-S batteries. Thermal treatment at reducing conditions and phosphorization of ZIF-67 were proposed to adorn the carbon NPs with CoP, which reduces the solubility of the polysulfides and inhibits them from escaping from the pores of the carbon-based material.

MOF-derived materials can fulfill comparable charge capacity requirements in Li-Se battery cathodes. ZIF-8 and MOF-5 were among the initial metal-organic frameworks utilized to generate porous carbon structures by direct pyrolysis for the purpose of accommodating polyselenides in lithium-selenium [162] batteries. A comparable method was employed to produce from an Al-MOF, rod-shaped N-doped carbon sponge characterized by a porous architecture capable of facilitating bulk transition of Se ions [163]. Researchers highlight the significance of doping with hetero atoms and the introduction of mesopores in layered carbonaceous materials for maintaining stable electrochemical performance of the cathode across 200 cycles, achieving a consistent capacity of 443.2 mAh g⁻¹ at 0.5 C.

Jin et al. [164] recently synthesized distinctive carbon nanosheets featuring pores measuring between 0.58 and 150 nm using the carbonization of SAF (Figure 7). The resulting nanomaterial offered a highly conductive matrix able to inhibit volume expansion due to Se/Li interactions, and the PCNS/Se cathode achieved up to 200 cycles at current rates ranging from 0.25 to 2 C.

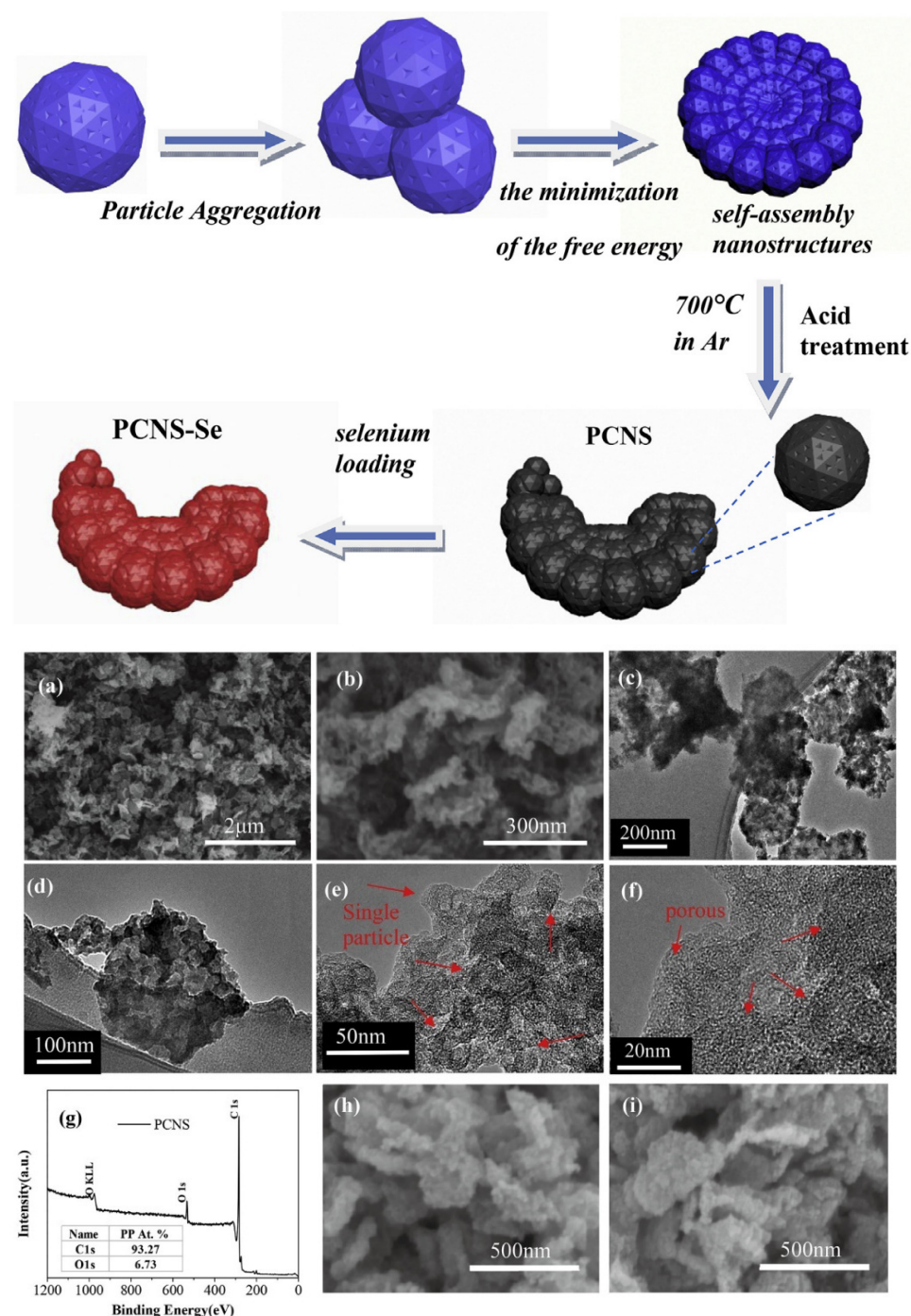


Figure 7. (top) Illustration of the synthesis route for the PCNS/Se composite. (bottom) (a,b) PCNS obtained by carbonizing SAF in N_2 atmosphere at $700\text{ }^\circ\text{C}$ for 1 h; (c,d) Low- and (e,f) high-magnification TEM images of the PCNS; (g) XPS survey spectrum of the PCNS; (h) SEM image of PCNS/Se-58 and (i) PCNS/Se-63 (Reproduced from [164] with permission).

The thermal treatment of MOFs has been documented as an effective method for synthesizing cathodes for metal-ion batteries based on metal oxides. As previously stated, in metal-ion batteries, the cathode in lithium-ion batteries is the electrode that contains lithium. Yin et al. [165] synthesized different $\text{LiNi}_{0.5}\text{Mn}_{1.5}\text{O}_4$ electrodes initially by a MOF thermal oxidation technique, subsequently employing conventional methods to evaluate their performance. The resulting M-LNMO exhibited improved structural characteristics that significantly boosted Li-ion cell efficiency. This behavior of the enhanced electrode is ascribed to the uniform distribution of materials, elevated crystallinity, and the removal

of contaminations. Metal oxides generated from MOFs (Mn_2O_3 and V_2O_5) have been utilized in cathodes for Zn-ion batteries to enhance the capacity for charge storage and rechargeability of the resulting devices [72,166].

2.4.3. Solid-State Lithium Batteries

Due to their potential for superior safety [167] and energy density, all-solid-state batteries are garnering growing attention as a leading candidate for future battery storage. Nonetheless, their extensive uses are constrained by several technological obstacles, such as low-conductivity electrolytes, dendritic formation [168], and inadequate cycle and/or rate performance [169]. They provide extremely high specific capacities at an increased electrochemical window, and thus enable very high energy densities. Despite the benefits provided by solid-state batteries, the used polymer electrolytes suffer from sluggish ion kinetics and inadequate selectivity in Li^+ diffusion. Furthermore, extensive research is necessary to fully understand how lithium metal anodes behave dependent on the operating conditions [170]. Polymer electrolytes, including polyethylene oxide (PEO) and polyvinylidene fluoride (PVDF), are advantageous because of their affordability, versatility in preparation, and superior interfacial wetting capacity. Nonetheless, the ionic conductivity remains constrained to the range of 10^{-6} – 10^{-7} S cm $^{-1}$ at ambient temperature [171].

MOFs are suggested as novel ingredients for solid-state electrolytes [172]; nonetheless, the development of functionalized MOFs and the comprehension of their impact on ion transportation have presented significant challenges [173]. The specific benefits of MOFs can be used to control diffusion paths by their high specific surface area as cation hopping centers are very close to each other, thereby enabling a fast cation movement at low activation energies [174]. Furthermore, the high ordering in MOF-crystals leads to the uniform distribution of metallic cations, and thus inhibits the formation of dendrites [175].

Wu and Guo [176] reported the preparation and utilization of UiO/Li-IL solid electrolytes, by incorporating Li-IL into the nanopores of UiO-66 metal-organic frameworks in LiFePO_4 /Li solid-state batteries. This type of solid electrolyte facilitates rapid lithium-ion migration in solid-state lithium batteries due to their high ionic conductivity (3.2×10^{-4} S cm $^{-1}$) and low interface resistances between the electrode and the solid electrolyte. The prepared batteries sustain 130.4 mAh g $^{-1}$ after 100 cycles at a rate of 0.2 C. Additionally, the initial discharge capacity recorded is 119 mAh g $^{-1}$, with a retention rate of 94% after 380 cycles at a rate of 1 C. To tackle the interface challenge and enhance energy density, Wang et al. [177] prepared an innovative solid-like electrolyte (SLE) utilizing ionic-liquid-impregnated MOF nanocrystals (Li-IL@MOF). This material exhibits remarkable electrochemical characteristics, featuring an excellent ionic conductivity of 3.0×10^{-4} S cm $^{-1}$, and strong compatibility between Li metal and active electrodes, resulting in low interfacial resistance.

Wang et al. [178] combined also ionic liquids but with 1,3,5-benzenetricarboxylic acid and copper complexes (HKUST-1) to create MOF arrangements, which were then incorporated into a PEO-based polymer, subsequently yielding CPE films by the solution casting process. The ionic conductivity of the synthesized CPEs film at 30 °C reached 1.20×10^{-4} S cm $^{-1}$, significantly surpassing that of the original PEO. Two-dimensional-copper p-dibenzoate (Cu(BDC)) MOFs, which possess sufficient open metal sites, have been used by Yu et al. [179] to prepare composite polymer electrolytes (CPEs) in a demonstration of engineering of fast conduction paths for lithium ions.

3. Metal-Organic Frameworks (MOFs) in Fuel Cells

Hydrogen fuel cells represent a superior alternative to fossil fuels, providing a clean and carbon-free means of transforming chemical energy directly into electrical energy [180].

Furthermore, they are almost twice as efficient as fossil fuels (more than 50% electrical efficiency for fuel cells versus ca. 30–35% for fossil fuels because of the losses of the Carnot cycle) [181,182]. They comprise two electrodes separated by a solid electrolyte. The electrodes must be catalytically active (especially in low temperature fuel cells) and possess a certain morphology and porosity that allows for the transport of reactants as close as possible to the electrode/electrolyte interface, and at the same time, the removal of reaction products (mostly water). Two significant obstacles impede the broad implementation of fuel cells. The first is related to mass transport limitations during the operation and the second is related to the risk of metal leaching from the catalytic materials used in the electrodes, which can result in a decreased lifespan [183]. A catalyst layer's elevated porosity is essential to optimize reactant accessibility to the active sites located on the surface of the micropores of the gas diffusion electrode as well as of the active (catalyst loaded) electrode. Mesoporous templates can facilitate the attainment of a more uniform pore size and an organized mesoporous structure, enhancing mass transfer and resulting in superior PEMFC performance. The morphology and pore structure of the catalyst significantly affect its overall efficiency in proton exchange membrane fuel cells (PEMFCs). It is important to reach a balance between the presence of micropores, where catalytic sites are situated, and mesopores that help in mass transport [184]. Carbonization of MOFs is an interesting and viable option to produce carbonaceous materials with high porosity [185]. The carbonization of metal-organic frameworks (MOFs) resulted in the formation of well-structured networks inside their framework, and hence enhancing mechanical and chemical stability [186]. A complex but controlled pore structure is essential for effective diffusion of reactants and products, reducing mass transport limitations, and thus extending PEMFCs long-term operability reaching practical applications [187].

Metal-organic frameworks (MOFs) have numerous benefits for electrocatalysis, electrolyte membranes, and hydrogen storage materials; they exhibit exceptional design flexibility, extensive surface-to-volume ratios, and permit surface and bulk modification by different functional groups with multivalent linkers and metallic centers to enhance affinity for fuel cell applications. Significant attempts have been undertaken to harness the distinctive features of MOFs as materials for high-performance fuel cells [12].

PEMFCs are regarded as efficient power sources for fuel cell electric cars due to their clean emissions, air purification capabilities, and superior durability [188]. The improvement in the fabrication of metal-organic frameworks (MOFs) for fuel cell applications can be classified into three distinct approaches: (1) oxygen reduction reaction (ORR) catalyst material [39,189–193], (2) hydrogen storage material [194–197], and (3) inorganic filler for proton exchange membranes (PEMs) [198–201] or stand-alone electrolyte membranes [202,203] even for high-temperature PEM fuel cells with polybenzimidazole as electrolyte material [204].

In the anode compartment of PEMs, the supplied hydrogen is oxidized to protons and delivers electrons, which are transferred to the cathode side where they are needed for the reduction in the oxygen (Figure 8).

The created protons traverse the polymeric membrane towards the cathode, where they react with the supplied O₂ gas to form water. The generated water is expelled from the catalyst surface into the flow-field channel due to capillary pressure differentials. Notwithstanding this water generation, the volume of water back-diffusion in a conventional PEM fuel cell is typically low, as the produced water is expelled externally (Figure 8b). MOFs provide superior water-storage capacity and demonstrate consistent performance due to their porous architecture and extensive surface [205]. Choi et al. [188] presented a water-stable Zr-based UiO-66-type MOF incorporating benzene-1,2,4,5-tetracarboxylate ligands, henceforth designated as UiO-66(Zr)-(COOH)₂, as a functional water-storage material for the cathode

catalyst layer of membrane electrode assemblies (MEAs) (Figure 8c). $\text{UiO-66}(\text{Zr})\text{-}(\text{COOH})_2$ exhibits thermal and electrochemical stability, hence ensuring robustness and endurance throughout the PEMFC operation. In this respect, Du et al. [206] have fabricated a series of composites by incorporating ionic liquid (IL) into chromium terephthalate MIL-101 using the ship-in-bottle method (IL@MIL-101). The resulting IL@MIL-101 exhibited high water retention, which is crucial for proton conduction in various energy-related applications at low relative humidity.

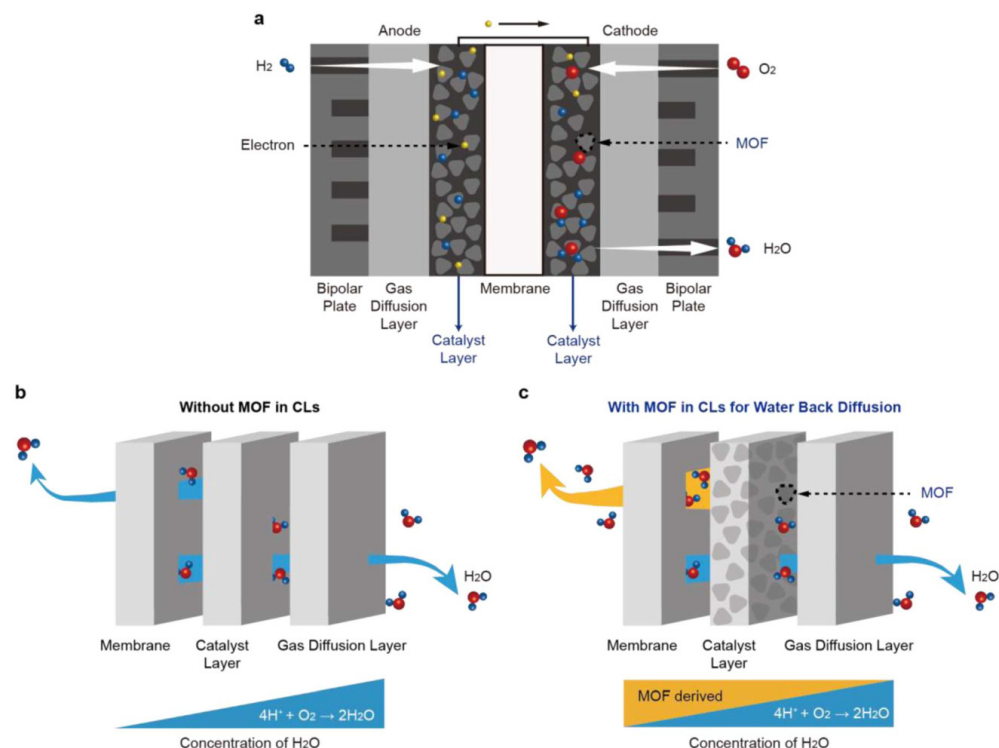


Figure 8. Influence of a metal-organic framework (MOF) on water back-diffusion in the cathode catalyst layer of a PEMFC. (a) Schematic illustrating the principle of PEMFC. (b) Pathways of water molecules in a catalyst layer (CL) without the MOF. (c) Water back-diffusion caused by the presence of MOF, which functions as a water reservoir in the catalyst layer (Reproduced from [188] with permission).

Besides the above-described fuel cells, microbial fuel cells (MFCs) are devices that generate electric energy while simultaneously treating wastewater, utilizing microorganisms as biocatalysts [207,208]. The microbial fuel cell (MFC) represents a technology that has demonstrated the capability to process a diverse range of substrates [209]. MFCs employ electrochemically active bacteria that oxidize an organic substrate while reducing an electron acceptor, leading to concurrent wastewater treatment and current generation [210]. Nonetheless, the utilization of MFCs is limited by the cathodic oxygen reduction reaction (ORR) because of its elevated energetic barrier and slow kinetics at room temperature [211]. Consequently, achieving elevated electrode potential and optimal energy output necessitates the development of highly efficient and stable metal-based ORR electrocatalysts, which is essential for the practical implementation of MFCs [212].

Besides the enzymatic anodic reaction, the most important and difficult reaction in microbial fuel cells is the cathodic oxygen reduction reaction (ORR). This reaction is similarly important for all fuel cells working at low temperatures. At present, platinum group metals are recognized as the leading catalysts for ORR. However, the scarcity of these resources and their associated high costs necessitate the exploration of alternative, cost-effective electrocatalysts [213].

Metal-organic frameworks (MOFs) combined with activated carbon demonstrated a significant enhancement in power density, surpassing activated carbon by 60% and platinum by 160% [214]. The nitrogen groups in the MOFs, specifically pyridine-N and pyrrole-N, contributed to an increase in active sites and a reduction in charge transfer impedance, thereby facilitating improved oxygen reduction reaction (ORR). Moreover, metal-organic frameworks (MOFs) diminish diffusion limitations by enhancing conductivity and charge transfer, thereby increasing electron transfer efficiency and improving power production. The addition of reduced graphene oxide (rGO) in various amounts to carbon black (CB) significantly improved cathodic performance. This composite demonstrated superior capacitance, electron transport, and cathodic polarization resistance [215,216].

In the following paragraphs, some recent works on the development of MOFs in PEM membranes, and ORR catalysts for PEM fuel cells as well as for microbial fuel cells are given.

3.1. Metal-Organic Frameworks (MOFs) for Proton Exchange Membrane Fuel Cell (PEMFC) Electrolyte Membranes

The polymer electrolyte is considered the key component of PEMFCs, as it facilitates proton conduction, separates the cathode and anode compartments, and inhibits the transport of electrons within the cell.

The incorporation of a proton-conducting metal-organic framework (PCMOF) by hybrid assembly with an ionomer can enhance membrane performance in proton exchange membrane fuel cell (PEMFC) applications [217].

Nafion® (DuPont Fuel Cells, Wilmington, NC, USA), a perfluorosulfonated polymer, is an excellent proton-conducting membrane, but suffers from the necessity to be watered. Because of the sulfonic groups, Nafion is hydrophilic and supports the H⁺ transport by promoting the Grotthuss proton hopping mechanism as the acidic groups act as a proton carrier [218]. Water absorption and ion-exchange capacity (IEC) are fundamental chemical properties of polymer electrolyte membranes.

To enhance the electrochemical performance of a Nafion membrane, Hou et al. [219] incorporated MOFs into the Nafion matrix. Zn-MOF and amino-modified Zn-MOF served as fillers in the produced hybrid membranes, with a content of 5% MOFs. At 80 °C and 58% relative humidity, the proton conductivities of the resulting Zn-MOF/Nafion-5 and Zn-MOF-NH₃/Nafion-5 were 7.29×10^{-3} S cm⁻¹ and 2.13×10^{-2} S cm⁻¹, outperforming Nafion by 1.87 times and 5.47 times, respectively. The proton conductivity of hybrid MOF-Nafion electrolyte membranes could be substantially increased using sulfonated MOFs in the polymer, imitating the same environment for the proton conduction mechanism [220].

Another interesting polymer for electrolyte membranes in so-called high-temperature PEMFCs is polybenzimidazole (PBI). It works in high-temperature PEMFCs ($T > 100$ °C) because of its elevated glass transition temperature [221]. As the working temperature is above 100 °C, it cannot be wetted with liquid water, and therefore phosphoric acid is used [222].

Summarizing this subsection, it can be stated that composite membranes created from metal-organic frameworks and polymers exhibit outstanding performance and innovative design concepts, indicating significant potential for commercial applications.

3.2. Oxygen Reduction Reaction (ORR) Catalysts for Proton Exchange Membrane (PEM) Fuel Cells

On the basis of previous works of Li et al. [223] and Wang et al. [224] on CoO/N/C (CoO supported on nitrogen-doped carbon), Zhang et al. [225] synthesized nano-catalysts based on N-doped C-encapsulated metal cobalt nanoparticles with a core-shell structure (Co@N/C-Joule) through pyrolysis of ZIF-67 in an argon atmosphere. An N-doped car-

bonaceous material sheet is applied to the surface of Co nanoparticles, creating a core-shell configuration. The slender carbon sheet protects the cobalt nanoparticles, thereby enhancing catalytic activity. By comparing samples synthesized via conventional furnace pyrolysis and those synthesized using CTS in either Ar or Air atmosphere, it was shown that the latter demonstrated a reduction in pyrolysis time by about four orders of magnitude and a decrease in carbon shell thickness from 3.3 nm to 1.3 nm, along with an improvement in electrochemical performance. The enhanced catalytic efficiency is ascribed to the nanoparticle size of the catalysts and the tiny nitrogen-doped carbon shell.

3.3. Oxygen Reduction Reaction (ORR) Catalysts for Microbial Fuel Cells

Catalysts in MFCs can be categorized as metal-free catalysts, noble-metal catalysts, non-noble metal catalysts (comprising metal-organic frameworks (MOFs) and covalent organic frameworks (COFs)), single atom catalysts, and biocatalysts (Figure 9) [226].

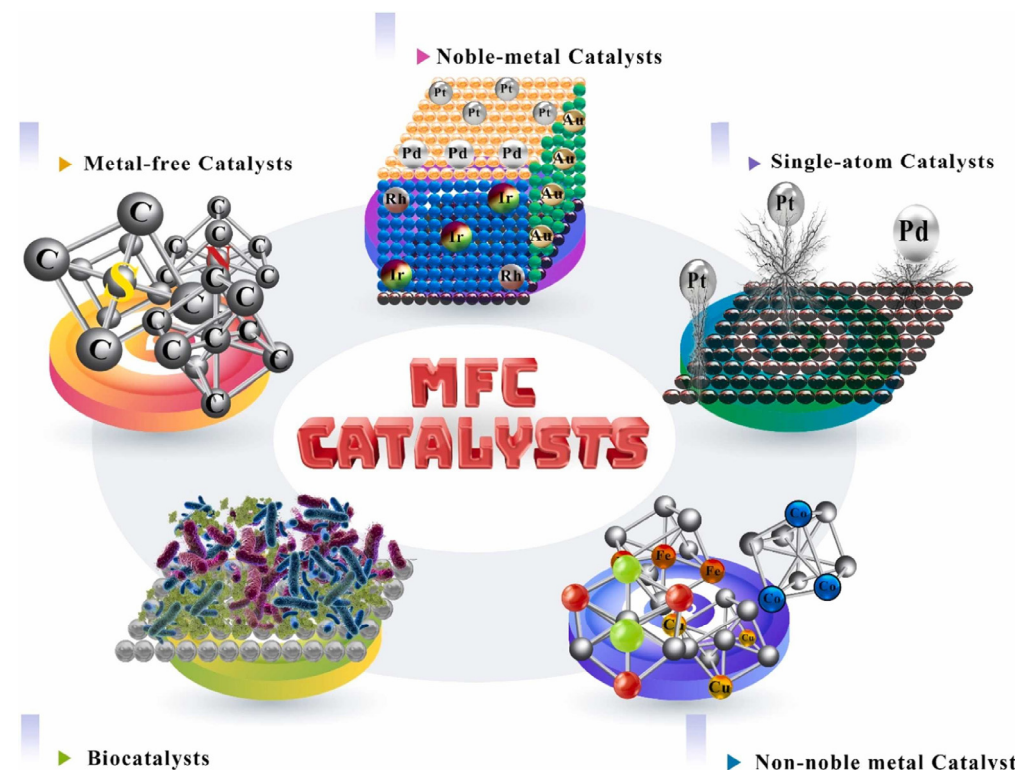


Figure 9. Different structures and materials that are applied in MFC as catalysts (Reproduced from [226] with permission).

Jiang et al. [211] established a mesoporous silica (mSiO_2)-assisted method for synthesizing highly distributed CuCo nanoalloys integrated into nitrogen-doped carbon Cu/Co-NC@mS catalyst, employing the zeolithic imidazolate framework (ZIF) as a source of carbon and nitrogen. The results indicate that protecting by mSiO_2 allows for preventing the aggregation of CuCo nanoalloys, thereby facilitating the formation of highly dispersed CuCo nanoparticles. The catalyst obtained by pyrolyzing at $800\text{ }^\circ\text{C}$ (Cu/Co-NC@mS-800) demonstrates superior ORR performance compared to other Cu/Co-NC@mS-T catalysts, exhibiting a maximum power density of 1000 mW m^{-2} when utilized as an air electrode in MFCs. The increased ORR performance of Cu/Co-NC@mS-800 was credited by the authors to several factors: (a) the presence of highly dispersed CuCo nanoalloy particles and an increased mesoporous surface area due to mSiO_2 protection; (b) the formation of a concave regular dodecahedron mesoporous structure supported by a thin graphitic carbon layer; (c) the synergistic effect observed between CuCo nanoalloys.

Based on density functional theory (DFT) calculations indicating that the interaction between Cu-BTC and MoS₂ markedly decreases charge transfer resistance and improves the oxygen reduction reaction (ORR), MoS₂ flower-like nanosheets were effectively incorporated onto a copper MOF (Cu-BTC) through a straightforward hydrothermal synthesis method, resulting in the formation of a Cu-BTC@MoS₂ composite material that was utilized as a cathode catalyst in microbial fuel cells (MFCs). The Cu-BTC@MoS₂ demonstrates a high limiting current density and exchange current density in the ORR, adheres to a four-electron transfer pathway, and exhibits significantly greater methanol tolerance compared to commercial Pt/C catalysts. The Cu-BTC@MoS₂-4 attained a peak power density of 241.20 mW m⁻². This performance is 9.89 times greater than that of pristine carbon cloth (CC), 3.58 times that of Cu-BTC, and 2.49 times that of MoS₂, while sustaining 328 mV during the entire operating time. The catalytically active material achieved a chemical oxygen demand (COD) removal of 94.89%, demonstrating considerable prospects for wastewater treatment applications [227]. Zeolitic imidazolate framework-67 (ZIF-67)-coated MoS₂ has been used as a low-price ORR catalyst in the cathode of microbial fuel cells exhibiting exceptional stability as well as electrocatalytic activity, mainly due to its high specific surface area of up to 1627.4 m²/g [228].

In Table 1, indicative performance metrics of representative MOF-based materials for rechargeable batteries and fuel cells are tabulated.

Table 1. Indicative performance metrics of representative MOF-based materials and derivatives for rechargeable batteries and fuel cells.

| MOFs | Derivatives/Devices | Discharge Capacity [mAh g ⁻¹ @ mA g ⁻¹ or @ C] | Cycle Performance [mAh g ⁻¹ @ Cycles] | Ref. |
|--|--|---|---|-------|
| Ni/Co-MOF | NiFe ₂ O@NiCo-LDH | 891.2 @ 500 | 636.9 @ 100 | [229] |
| Ni-Co-BTC MOF | NixCo _{3-x} O ₄ | 1619.2 @ 1000 | 832 @ 673 | [230] |
| Zn-Co PBA | Co ₃ O ₄ /NiO-C | 864 @ 1000 | 776 @ 1000 | [231] |
| ZIF-67, red P | Co _x P-NC-800 | 2450 @ 1000 | 550 @ 100 | [232] |
| MOF-74 | MnCo-MOF | 11,150 @ 200 | 1000 @ 44 | [133] |
| ZIF-67 | NiCo ₂ O ₄ /NiO | 1535 @ 200 | 1492 @ 100 | [233] |
| [Mn(phen)H ₂ O] [V ₂ O ₆] | MnV ₂ O ₄ /C | 400 @ 100 | 377 @ 1000 | [234] |
| MIL-125(Ti) | LiNi _{0.5} Co _{0.2} Mn _{0.3} O ₂ | 186.7 @ 1000 | 145.3 @ 100 | [235] |
| ZIF-8 | S@S-NOHPC | 927.7 @ 200 | 367 @ 200 | [236] |
| CoPC | CoPC@GO | 938 @ 1 C | 919 @ 250 | [237] |
| ZIF-8 | Co-NC@AZO/S | 1206.2 @ 200 | 950.03 @ 500 | [238] |
| ZIF-8@ZIF-67 | ZnSe@CoSe@CN | 2739 @ 100 | 1500 @ 100 | [239] |
| Zn-Co PBA | ZnO/Co ₃ ZnC | 1163.9 @ 200 | 1162.4 @ 300 | [240] |
| Mn-MOF | MnO@rGO | 1412.2 @ 2000 | 920 @ 160 | [241] |
| Ni-Co NTA | NiCo ₂ O ₄ | 3158 @ 100 | 1310 @ 100 | [242] |
| ZIF-8 | S@CuIr/NC | 1288 @ 0.2 C | 689 @ 500 | [243] |
| ZIF-8 | CNT-NC@GC/S | 1498 @ 0.1 C | 743 @ 500 | [244] |
| UiOSOL | LiFePO ₄ /Li metal | 161 @ 0.1 C | 155 @ 600 | [245] |
| MOF-801 | NCM811/Li metal | 179 @ 0.5 C | 113 @ 400 | [246] |
| [NH ₂ (CH ₃) ₂] [Fe _{III} Fe _{II} (HCOO) ₆] | Fe ₃ O ₄ @C | 1714 @ 100 | 1041 @ 50 | [247] |
| Co-BDC nanoplates | Co ₃ O ₄ nanosheets | 961 @ 1000 | 775 @ 200 | [248] |
| Fe-Ni-BDC MOF | NixFe _{3-x} O ₄ nanotubes | 1466 @ 250 | 1184 @ 200 | [249] |
| Fe-NTA | V-FeP | 1228.3 @ 100 | 590.7 @ 1000 | [250] |
| CAU-1-NH2 | CAU-1-NH2-PMMA | 1480 @ 200 | 450 @ 66 | [251] |

4. Limitations and Outlook

Traditional MOFs exhibit significant limitations, notably in terms of conductivity and structural integrity, which restrict their utilization in electrochemical applications. Specific challenges associated with MOFs must be addressed to facilitate their wider commercialization. The limited electrochemical conductivity significantly constrains their potential applications, leading to the design of various nanocomposites with diverse structural forms across different dimensionalities. A viable alternative is to integrate MOFs with carbon materials, such as carbon nanotubes with superior conductivity, or to create binary metal oxides.

The functionalization of MOF variants remains limited; nonetheless, substantial potential exists to enhance their electrochemical properties. This can be accomplished by enclosing functional groups and various species within their frameworks, with the objective of developing high-performance energy storage devices through the identification of suitable MOF derivatives for both anodes and cathodes in electrochemical devices. MOF derivatives have emerged as effective materials to overcome these limitations and investigate applications across diverse electrochemical domains. Those substances perform as powerful templates, allowing for accurate control over the shape, chemical manipulation, heteroatom doping, increased surface area, and structural alterations. Significant potential exists for future applications, warranting increased interest from the academic community.

Future exploration in metal-organic frameworks (MOFs) may shift the focus from conventional applications like storage and separation to more critical concerns, including the production of clean energy. Significant advancements have been achieved in enhancing the performance of MOF-based components to meet industrial and commercial standards. Further progress necessitates that MOFs exceed the benchmarks established by conventional materials.

We do not yet have a clear grasp of the nature of conductivity in MOFs. Understanding how low-energy charge transport channels may be established in MOFs at the atomistic level will significantly speed up the creation of exceptional conductive MOFs. Computational quantum mechanical techniques can generate detailed information on the electronic structure in this situation with enough precision to shed light on the conductive behavior of MOFs. Using machine learning to speed up the screening and discovery of novel conductive materials is a new alternative design technique.

The integration of MOFs in energy production devices stands for a growing frontier, leading to bright outcomes. However, there are significant obstacles that require attention, such as the Ion Conduction Mechanism, the mechanistic investigation of which remains in the early stages, requiring comprehensive theoretical and fundamental analysis.

Furthermore, MOFs exhibit adjustable characteristics, including pore dimensions, structural configurations, crystal-size, and crystal-structure [252]. A thorough examination of the systematic relationships between these changes and their corresponding electrochemical characteristics is necessary. In this respect, the four-dimensional analysis system of “structure-performance-mechanism-application” [253–260] can be applied to improve the quality and efficiency of the developed MOF-based composite materials. An excellent overview on the application of this analysis system on lithium-ion batteries is given by Ji et al. [261].

Highlighting the use of inexpensive raw materials and implementing economically viable synthesis methods can improve the commercial feasibility of MOF-sourced solid electrolytes [28].

Yuan et al. [32] highlighted the absence of systematic research about the correlation between the synthesis process and the composition and structure of MOFs and their associated materials, complicating the understanding of the physicochemical alterations

that transpire during synthesis. Using high-temperature *in situ* methodologies may be a viable pathway to examine this issue.

The materials derived from MOFs exhibit significant potential and various benefits for use in energy production and storage systems. Despite the numerous complex challenges that are difficult to address in the short term, there is a strong conviction that a promising future lies ahead for these innovative materials based on MOFs in real-world applications.

5. Summary

This review concludes with recent advancements in MOF-based materials for rechargeable batteries and fuel cells. This study emphasizes the impact of various synthesis strategies on the morphologies and sizes of these materials, demonstrating the significant potential of metal-organic frameworks (MOFs) to improve electrochemical devices for energy storage, such as rechargeable batteries, and energy production, including fuel cells. The relationship between electrochemical performance and the morphology of electrode active materials is emphasized. The primary challenges and perspectives concerning materials derived from MOFs for practical and sustainable electrochemical energy conversion applications are succinctly discussed.

Metal-organic frameworks (MOFs) demonstrate significant versatility, enabling systematic modifications designed to address diverse emerging requirements. In this context, metal-organic frameworks (MOFs) can significantly contribute to the hydrogen economy through their applications in electrocatalysis for hydrogen production and oxygen reduction, proton exchange membranes (PEMs), and energy storage, including rechargeable batteries and supercapacitors.

MOFs are compelling alternatives for fuel cell technologies due to their adaptable structures, diverse chemistry, highly uniform pores, adjustable pore morphologies, and high surface areas (up to $5.0 \times 10^3 \text{ m}^2 \text{ g}^{-1}$). Additionally, the rational tuning of MOF properties has been facilitated by the meticulous design and functionalization of MOFs, which has been made possible by the use of multifunctional bridging ligands and post-synthetic modifications. The potential for the application of MOFs in fuel cells is indicated by the extensive variety of possible combinations of metal centers and organic linkers. The potential for a systematic investigation into the impact of structural parameters and chemical compositions on the performance of MOF-based electrochemical devices and the ability to manipulate pore structures in conjunction with surface engineering could provide significant fundamental insights.

A substantial body of research on MOFs and their derivatives has confirmed the reliability of their structures and chemical characteristics for contemporary electrochemical applications at the laboratory scale. However, further developments are necessary, as several problems with MOF-based electrochemical devices are presently being faced and require immediate attention for a successful upscaling of the use of MOFs in electrochemical energy production and storage devices.

Author Contributions: Conceptualization, C.A. and G.S.; validation, C.A., N.A. (Nikolaos Argirasis), N.A. (Niyaz Alizadeh), and G.S.; investigation, C.A. and M.-E.K.; data curation, C.A.; writing—original draft preparation, C.A. and N.A. (Nikolaos Argirasis); writing—review and editing, C.A., N.A. (Nikolaos Argirasis), N.A. (Niyaz Alizadeh), and M.-E.K.; supervision, C.A. and G.S.; project administration, G.S. All authors have read and agreed to the published version of the manuscript.

Funding: This research received no external funding.

Data Availability Statement: No new data have been produced for this work.

Conflicts of Interest: Authors Christos Argirasis, Niyaz Alizadeh and Nikolaos Argirasis were employed by the company mat4nrg—Gesellschaft für Materialien und Energieanwendungen mbH.

The remaining authors declare that the research was conducted in the absence of any commercial or financial relationships that could be construed as a potential conflict of interest.

References

1. DNV As, Norway. Energy Transition Outlook 2024—A Global and Regional Forecast to 2050. Available online: www.dnv.com (accessed on 20 April 2025).
2. Ahmed, S.; Ali, A.; Asif, M.; Shim, J.; Park, G. Exploring innovative trends and advancements in rechargeable zinc-air batteries. *Inorg. Chem. Commun.* **2024**, *170*, 113288. [[CrossRef](#)]
3. Hu, X.; Li, J.; Zhou, H.; He, Z.; Liang, H.; Ou, W.; Chung, L.-H.; He, J. Ligand engineering of metal-organic frameworks as efficient electrocatalysts for wide-temperature lithium-sulfur batteries. *J. Power Sources* **2025**, *629*, 236053. [[CrossRef](#)]
4. Kim, D.; Park, Y.; Nam, K.W. Inhibiting polysulfide shuttle and enhancing polysulfide redox: Conductive 2D metal-organic framework coated separators for lithium-sulfur batteries. *J. Alloys Compd.* **2024**, *1009*, 176812. [[CrossRef](#)]
5. Sun, Y.; Zhang, Y.; Chen, Z.; Li, C.; Duan, C.; Kawi, S.; Li, Y. Construction of amino functional metal-organic framework modified aramid composite separators with high Li⁺ transport channels for dendrite-free lithium-ion batteries. *J. Colloid Interface Sci.* **2025**, *683*, 262–273. [[CrossRef](#)]
6. Zou, M.; Dong, M.; Zhao, T. Advances in metal-organic frameworks MIL-101(Cr). *Int. J. Mol. Sci.* **2022**, *23*, 9396. [[CrossRef](#)]
7. Kitagawa, S.; Kitaura, R.; Noro, S. Functional Porous Coordination Polymers. *Angew. Chem. Int. Ed.* **2004**, *43*, 2334–2375. [[CrossRef](#)]
8. Yaghi, O.M.; O’Keeffe, M.; Ockwig, N.W.; Chae, H.K.; Eddaoudi, M.; Kim, J. Reticular synthesis and the design of new materials. *Nature* **2003**, *423*, 705–714. [[CrossRef](#)]
9. Li, J.X.; Bao, T.; Zhang, C.; Song, H.; Zou, Y.Y.; Yuan, I.; Xi, Y.; Yu, C.Z.; Liu, C. A general strategy for direct growth of yolk-shell MOF-on-MOF hybrids. *Chem. Eng. J.* **2023**, *472*, 144926. [[CrossRef](#)]
10. Arbulu, R.C.; Jiang, Y.B.; Peterson, E.J.; Qin, Y. Metal-organic framework (MOF) nanorods, nanotubes, and nanowires. *Angew. Chem. Int. Ed.* **2018**, *57*, 5813–5817. [[CrossRef](#)]
11. Furukawa, H.; Cordova, K.E.; O’Keeffe, M.; Yaghi, O.M. The Chemistry and Applications of Metal-Organic Frameworks. *Science* **2013**, *341*, 974. [[CrossRef](#)]
12. Lei, L.; Cheng, Y.; Chen, C.; Kosari, M.; Jiang, Z.; He, C. Taming structure and modulating carbon dioxide (CO₂) adsorption isosteric heat of nickel-based metal organic framework (MOF-74(Ni)) for remarkable CO₂ capture. *J. Colloid. Interface Sci.* **2022**, *612*, 132–145. [[CrossRef](#)] [[PubMed](#)]
13. Zhang, W.; Bojdys, M.J.; Pinna, N. A universal synthesis strategy for tunable metal-organic framework nanohybrids. *Angew. Chem. Int. Ed.* **2023**, *62*, e202301021. [[CrossRef](#)] [[PubMed](#)]
14. Ren, Y.; Chia, G.H.; Gao, Z. Metal—Organic frameworks in fuel cell technologies. *Nano Today* **2013**, *8*, 577–597. [[CrossRef](#)]
15. Li, H.I.; Eddaoudi, M.; Keeffe, M.O.; Yaghi, O.M. Design and synthesis of an exceptionally stable and highly porous metal-organic framework. *Nature* **1999**, *402*, 276–279. [[CrossRef](#)]
16. Kumar, R.S.; Kumar, S.S.; Kulandainathan, M.A. Efficient electrosynthesis of highly active Cu₃(BTC)₂-MOF and its catalytic application to chemical reduction. *Microporous Mesoporous Mater.* **2013**, *168*, 57–64. [[CrossRef](#)]
17. Kaur, G.; Kandwal Komal, P.; Sud, D. Sonochemically synthesized Zn (II) and Cd (II) based metal-organic frameworks as fluoroprobes for sensing of 2,6-dichlorophenol. *J. Solid. State Chem.* **2023**, *319*, 123833. [[CrossRef](#)]
18. Glowniak, S.; Szczesniak, B.; Choma, J.; Jaroniec, M. Recent developments in sonochemical synthesis of nanoporous materials. *Molecules* **2023**, *28*, 2639. [[CrossRef](#)]
19. Mendes, R.F.; Rocha, J.; Almeida Paz, F.A. Chapter 8—Microwave Synthesis of Metal-Organic Frameworks. In *Metal-Organic Frameworks for Biomedical Applications*; Mozafari, M.B.T., Ed.; Woodhead Publishing: Sawston, UK, 2020; pp. 159–176. [[CrossRef](#)]
20. Kumari, P.; Kareem, A.; Jhariat, P.; Kumar, S.; Panda, T. Phase purity regulated by mechano-chemical synthesis of metal-organic frameworks for the electrocatalytic oxygen evolution reaction. *Inorg. Chem.* **2023**, *62*, 3457–3463. [[CrossRef](#)]
21. Wang, W.P.; Chai, M.; Zulkifli, M.Y.B.; Xu, K.J.; Chen, Y.L.; Wang, L.Z.; Chen, V.; Hou, J.W. Metal-organic framework composites from a mechanochemical process. *Mol. Syst. Des. Eng.* **2023**, *8*, 560–579. [[CrossRef](#)]
22. Vaitsis, C.; Kanellou, E.; Pandis, P.K.; Papamichael, I.; Sourkouni, G.; Zorpas, A.A.; Argirasis, C. Sonochemical synthesis of zinc adipate Metal-Organic Framework (MOF) for the electrochemical reduction of CO₂: MOF and circular economy potential. *Sustain. Chem. Pharm.* **2022**, *29*, 100786. [[CrossRef](#)]
23. Muzaffar, N.; Afzal, A.M.; Hegazy, H.H.; Iqbal, M.W. Recent advances in two-dimensional metal-organic frameworks as an exotic candidate for the evaluation of redox-active sites in energy storage devices. *J. Energy Storage* **2023**, *64*, 107142. [[CrossRef](#)]
24. Zhang, G.; Jin, L.; Zhang, R.; Bai, Y.; Zhu, R.; Pang, P. Recent advances in the development of electronically and ionically conductive metal-organic frameworks. *Coord. Chem. Rev.* **2021**, *439*, 213915. [[CrossRef](#)]
25. Deng, F.; Zhang, Y.; Yu, Y. Conductive Metal-Organic Frameworks for Rechargeable Lithium Batteries. *Batteries* **2023**, *9*, 109. [[CrossRef](#)]

26. Lee, S.J.; Telfer, S.G. Multicomponent metal-organic frameworks. *Angew. Chem. Int. Ed.* **2023**, *62*, e202306341. [[CrossRef](#)]
27. Lin, Z.X.; Richardson, J.J.; Zhou, J.J.; Caruso, F. Direct synthesis of amorphous coordination polymers and metal-organic frameworks. *Nat. Rev. Chem.* **2023**, *7*, 273–286. [[CrossRef](#)] [[PubMed](#)]
28. Liu, M.; Liu, T.; Xu, J.; Shao, L.; Shi, X.; Sun, Z. Metal-organic frameworks based solid-state electrolytes for lithium metal batteries: Modifications and future prospects. *Next Energy* **2025**, *6*, 100191. [[CrossRef](#)]
29. Ajpi, C.; Leiva, N.; Lundblad, A.; Lindbergh, G.; Cabrera, S. Synthesis and spectroscopic characterization of Fe³⁺-BDC metal organic framework as material for lithium ion batteries. *J. Mol. Struct.* **2023**, *1272*, 134127. [[CrossRef](#)]
30. Guo, W.; Fu, Y. A perspective on energy densities of rechargeable Li-S batteries and alternative sulfur-based cathode materials. *Energy Environ. Mater.* **2018**, *1*, 20–27. [[CrossRef](#)]
31. Ullah, A.; Majid, A.; Rani, N. A review on first principles based studies for improvement of cathode material of lithium ion batteries. *J. Energy Chem.* **2018**, *27*, 219–237. [[CrossRef](#)]
32. Yuan, T.; Qi, S.; Ye, L.; Zhao, Y.; Jiang, Y.; Feng, Z.; Zhu, J.; Dai, L.; Wang, L.; He, Z. Metal-organic frameworks-based materials: A feasible path for redox flow battery. *Coord. Chem. Rev.* **2025**, *531*, 216503. [[CrossRef](#)]
33. Naseer, M.; Siyal, S.H.; Najam, T.; Afzal, S.; Iqbal, R.; Ismail, M.A.; Rauf, A.; Ahmad Shah, S.S.; Nazir, M.A. Engineering of metal oxide integrated metal organic frameworks (MO@MOF) composites for energy and environment sector. *Mater. Sci. Eng. B* **2025**, *313*, 117909. [[CrossRef](#)]
34. Boukayouht, K.; Bazzi, I.; Hankari, S.E. Sustainable synthesis of metal-organic frameworks and their derived materials from organic and inorganic wastes. *Coord. Chem. Rev.* **2023**, *478*, 214986. [[CrossRef](#)]
35. Zhang, Q.; Yan, S.G.; Yan, X.T.; Lv, Y. Recent advances in metal-organic frameworks: Synthesis, application and toxicity. *Sci. Total Environ.* **2023**, *902*, 165944. [[CrossRef](#)]
36. Connolly, B.M.; Mehta, J.P.; Moghadam, P.Z.; Wheatley, A.E.H.; Fairen-Jimenez, D. From synthesis to applications: Metal-organic frameworks for an environmentally sustainable future. *Curr. Opin. Green Sustain. Chem.* **2018**, *12*, 47–56. [[CrossRef](#)]
37. Vaitsis, C.; Sourkouni, G.; Argiris, C. Metal organic frameworks (MOFs) and ultrasound: A review. *Ultrason. Sonochem.* **2019**, *52*, 106–119. [[CrossRef](#)]
38. Esmaeili, M.S.; Mehrpooya, M.; Ganjali, M.R. Three-dimensional nanocomposites derived from combined metal organic frameworks doped with Ce, La, and Cu as a bifunctional electrocatalyst for supercapacitors and oxygen reduction reaction. *Int. J. Hydrogen Energy* **2025**, *97*, 483–500. [[CrossRef](#)]
39. Wang, H.; Jiang, L.; Chen, J.; Fu, M.; Diao, Z.; Liu, H.; Guo, H. Enhanced bioelectrochemical performance caused by porous metal-organic framework MIL-53(Fe) as the catalyst in microbial fuel cells. *Process Biochem.* **2020**, *99*, 147–153. [[CrossRef](#)]
40. Li, X.; Zheng, S.; Jin, L.; Li, Y.; Geng, P.; Xue, H.; Pang, H.; Xu, Q. Metal-organic framework-derived carbons for battery applications. *Adv. Energy Mater.* **2018**, *8*, 1800716. [[CrossRef](#)]
41. Wang, L.; Han, Y.; Feng, X.; Zhou, J.; Qi, P.; Wang, B. Metal-organic frameworks for energy storage: Batteries and supercapacitors. *Coord. Chem. Rev.* **2016**, *307*, 361–381. [[CrossRef](#)]
42. Talukder, N.; Wang, Y.; Nunna, B.B.; Lee, E.S. N-Doped Graphene (N-G)/MOF(ZIF-8)-Based/ Derived Materials for Electrochemical Energy Applications: Synthesis, Characteristics, and Functionality. *Batteries* **2024**, *10*, 47. [[CrossRef](#)]
43. Chen, Y.; Li, S.; Li, C.; Leng, X.; Prakash, N.G.; Ko, T.J. Functional La@ZIF-8-enhanced composite quasi-solid electrolyte for high-performance Li-metal batteries. *Chem. Eng. J.* **2025**, *508*, 160932. [[CrossRef](#)]
44. Chen, G.; Jin, B.; Sun, S.; Jiang, Q. Surface-functionalized metal-organic framework with high specific surface area optimizing composite solid electrolyte for high-performance solid-state lithium metal batteries. *Chem. Eng. J.* **2024**, *501*, 157704. [[CrossRef](#)]
45. Wang, L.; Zhu, G.; Lin, Y.; Wang, Y.; Zhu, Q.; Dai, Z. MOF-derived hierarchical porous carbon octahedrons for aluminum-ion batteries. *Carbon* **2023**, *202*, 305–313. [[CrossRef](#)]
46. Xu, K.; Bao, H.; Tang, C.; Maliutina, K.; Li, F.; Fan, L. Engineering hierarchical MOFs-derived Fe-N-C nanostructure with improved oxygen reduction activity for zinc-air battery: The role of iron oxide. *Mater. Today Energy* **2020**, *18*, 100500. [[CrossRef](#)]
47. Kori, A.H.; Khan, M.; Soylak, M. Metal organic framework composite (Ti₃AlC₂ @ZIF-67) for vortex assisted solid phase extraction of lead from water and food samples. *J. Food Compos. Anal.* **2024**, *125*, 105810. [[CrossRef](#)]
48. Javadian, S.; Moslemi, M.; Gharibi, H.; Parviz, Z.; Dalir, N.; Zeinodiny, A. Development and evaluation of a dual silica structure integrated with a metal-organic framework as a fast-charging anode for future lithium-ion batteries. *J. Power Sources* **2025**, *629*, 235974. [[CrossRef](#)]
49. Han, H.; Chao, S.; Bai, Z.; Wang, X.; Yang, X.; Qiao, J.; Chen, Z.; Yang, L. Metal-organic-framework-derived Co nanoparticles deposited on N-doped bimodal mesoporous carbon nanorods as efficient bifunctional catalysts for rechargeable zinc-air batteries. *Chemelectrochem* **2018**, *5*, 1868–1873. [[CrossRef](#)]
50. Mirandona-Olaeta, A.; Goikolea, E.; Lanceros-Mendez, S.; Fidalgo-Marijuan, A.; Ruiz de Larramendi, I. Ionic Liquid-Laden Zn-MOF-74-Based Solid-State Electrolyte for Sodium Batteries. *Batteries* **2023**, *9*, 588. [[CrossRef](#)]

51. Hassan, H.; Sunny, M.A.; Iqbal, M.W.; Afzal, A.M.; Yaseen, T.; Mohammad, S.; Alotaibi, N.H.; Manzoor, M.; Ismayilova, N.A. Innovative Si@MOF-5@CNT hybrid: Tailoring energy storage and catalysis in batteries, supercapacitors, and hydrogen evolution. *Diam. Relat. Mater.* **2024**, *148*, 111507. [[CrossRef](#)]
52. Zhou, Q.; Xia, C.; Li, J.; Cheng, A.; Liu, J.; Liu, H.; Li, L.; Wang, S. Sulfur-doped porous carbon derived by metal-organic framework (MOF-5) for high lithium/sodium storage performance. *Solid. State Ion.* **2024**, *411*, 116553. [[CrossRef](#)]
53. Wu, D.; Guo, Z.; Yin, X.; Pang, Q.; Tu, B.; Zhang, L.; Wang, Y.G.; Li, Q. Metal-organic frameworks as cathode materials for Li-O₂ batteries. *Adv. Mater.* **2014**, *26*, 3258–3262. [[CrossRef](#)] [[PubMed](#)]
54. Zhou, X.; Li, J.; Dong, H.; Luo, Y.; Liu, C.; Huang, Y.; Lai, X.; Huang, X.; Yue, B. MIL-53(Fe) anode for lithium-ion batteries with the capacity self-activation effect based on electrochemically induced crystalline-to-amorphization transformation. *Mater. Today Commun.* **2024**, *38*, 108200. [[CrossRef](#)]
55. Wang, Z.; Li, B.; Shao, F.; Zhang, S.; Shi, B.; Jing, Y.; Zou, X.; Jia, Y. Mechanistic insights into lithium-ion adsorption and isotope separation on ligand-tuned aluminum-based metal-organic frameworks. *Chem. Eng. J.* **2025**, *504*, 159061. [[CrossRef](#)]
56. Zhou, J.; Li, R.; Fan, X.; Chen, Y.; Han, R.; Li, W.; Zheng, J.; Wang, B.; Li, X. Rational design of a metal-organic framework host for sulfur storage in fast, long-cycle Li-S batteries. *Energy Environ. Sci.* **2014**, *7*, 2715–2724. [[CrossRef](#)]
57. Sondermann, L.; Smith, Q.; Strothmann, T.; Vollrath, A.; Beglau, T.H.J.; Janiak, C. Mechanochemical synthesis and application of mixed-metal copper-ruthenium HKUST-1 metal-organic frameworks in the electrocatalytic oxygen evolution reaction. *RSC Mechanochem.* **2024**, *1*, 296–307. [[CrossRef](#)]
58. Baumann, A.E.; Aversa, G.E.; Roy, A.; Falk, M.L.; Bedford, N.M.; Thoi, V.S. Promoting sulfur adsorption using surface Cu sites in metal-organic frameworks for lithium sulfur batteries. *J. Mater. Chem.* **2018**, *6*, 4811–4821. [[CrossRef](#)]
59. Liu, Z.; Kai Liu, K.; Zhi, K.; Luo, J.; Hu, Z.; Zhang, Y. A spontaneous spatial network structural metal-organic framework composite polymer electrolytes with excellent lithium transport performance for dendrite-suppressing lithium metal batteries. *Chem. Eng. J.* **2025**, *504*, 158820. [[CrossRef](#)]
60. Wang, S.; Liu, Y.; He, L.; Sun, Y.; Huang, Q.; Xu, S.; Qiu, X.; Wei, T. A gel polymer electrolyte based on IL@NH₂-MIL-53 (Al) for high-performance all-solid-state lithium metal batteries. *Chin. J. Chem. Eng.* **2024**, *69*, 47–55. [[CrossRef](#)]
61. Liu, Z.; Zhang, X.; Luo, J.; Yu, Y. Application of metal-organic frameworks to the anode interface in metal batteries. *Chin. Chem. Lett.* **2024**, *35*, 109500. [[CrossRef](#)]
62. Yan, J.; Zheng, X.; Wei, C.; Sun, Z.; Zeng, K.; Shen, L.; Sun, J.; Rümmeli, M.H.; Yang, R. Nitrogen-doped hollow carbon polyhedron derived from salt-encapsulated ZIF-8 for efficient oxygen reduction reaction. *Carbon* **2021**, *171*, 320–328. [[CrossRef](#)]
63. Yamada, T.; Shiraiishi, K.; Kitagawa, H.; Kimizuka, N. Applicability of MIL-101(Fe) as a cathode of lithium ion batteries. *Chem. Commun.* **2017**, *53*, 8215–8218. [[CrossRef](#)] [[PubMed](#)]
64. Vallem, S.; Song, S.; Oh, Y.; Kim, J.; Li, M.; Li, Y.; Cheng, X.; Bae, J. Designing a Se-intercalated MOF/MXene-derived nanoarchitecture for advancing the performance and durability of lithium-selenium batteries. *J. Colloid. Interface Sci.* **2024**, *665*, 1017–1028. [[CrossRef](#)] [[PubMed](#)]
65. Ai, C.; Yang, Z.; Shi, G.; Xue, Y.; Dai, H.; Yi, Q.; Fang, C.; Han, J. Increment entropy promoted small-polaron breakdown in metal-organic frameworks for sodium-ion batteries. *Chem. Eng. J.* **2024**, *500*, 157006. [[CrossRef](#)]
66. Chen, W.; Kang, T.; Lao, Z.; Cai, J.; Yang, W.; Zou, H.; Chen, S. Towards improved P2-type Na_{0.67}Ni_{0.5}Mn_{0.5}O₂ with fast Na ion diffusion via a metal organic framework coating for sodium ion batteries. *J. Energy Storage* **2025**, *109*, 115151. [[CrossRef](#)]
67. Xie, X.; Zhai, Z.; Cao, W.; Dong, J.; Li, Y.; Hou, Q.; Du, G.; Wa, J.; Tian, L.; Zhang, J.; et al. Bifunctional ligand Co metal-organic framework derived heterostructured Co-based nanocomposites as oxygen electrocatalysts toward rechargeable zinc-air batteries. *J. Colloid Interface Sci.* **2024**, *664*, 319–328. [[CrossRef](#)]
68. Zhang, H.; Cui, Y.; Li, R.; Peng, X.; Ren, P.; Liu, A.; Wen, S.; Qin, J.; Zhang, J.; An, M.; et al. Metal-organic framework derived phosphide-hydroxide heterostructure as bifunctional oxygen electrocatalyst for zinc-air batteries. *Alloys Compd.* **2024**, *976*, 173237. [[CrossRef](#)]
69. Vayenas, M.; Vaitisis, C.; Sourkouni, G.; Pandis, P.K.; Argirasis, C. Investigation of alternative materials as bifunctional catalysts for electrochemical applications. *Chim. Techno Acta* **2019**, *6*, 120–129. [[CrossRef](#)]
70. Liu, C.; Wu, B.; Liu, T.; Zhang, Y.; Cui, J.; Huang, L.; Tan, G.; Zhang, L.; Su, Y.; Wu, F. Metal-organic frameworks and their composites for advanced lithium-ion batteries: Synthesis, progress and prospects. *J. Energy Chem.* **2024**, *89*, 449–470. [[CrossRef](#)]
71. Naskar, I.; Naskar, S.; Kaur, B.; Ghosal, P.; Deepa, M. MIL-53(Al) metal-organic framework/carbon nanofibers and Al-nanoflakes/carbon composites for a stable Al-battery. *J. Energy Storage* **2024**, *77*, 109956. [[CrossRef](#)]
72. Mao, M.; Wu, X.; Hu, Y.; Yuan, Q.; He, Y.-B.; Kang, F. Charge storage mechanism of MOF-derived Mn₂O₃ as high performance cathode of aqueous zinc-ion batteries. *J. Energy Chem.* **2021**, *52*, 277–283. [[CrossRef](#)]
73. Zhu, Q.; Sun, W.; Zhou, H.; Mao, D. A Review of Lithium–Sulfur Batteries Based on Metal–Organic Frameworks: Progress and Prospects. *Batteries* **2025**, *11*, 89. [[CrossRef](#)]

74. Wang, D.; Zhao, X.; Yin, D.; Mi, D.; Qu, C.; Feng, M. Metal-Organic Frameworks derived Pr₂O₃-doped porous carbon nanosheets as efficient adsorption-catalytic separator coating materials for lithium-sulfur batteries. *J. Power Sources* **2025**, *635*, 236540. [[CrossRef](#)]
75. Xiao, Y.; Qi, C.; Yang, D.; Ma, D.; Huang, S. Toward high performance Lithium-Sulfur batteries based on Metal-Organic Frameworks: Progress and prospects. *Mater. Sci. Eng. B* **2025**, *313*, 117983. [[CrossRef](#)]
76. Zhao, T.; Chen, J.; Xiao, P.; Nie, S.; Luo, F.; Chen, Y. Exploring metal-organic frameworks in battery electrodes, separators, and electrolytes: A comprehensive review. *Coord. Chem. Rev.* **2025**, *532*, 216501. [[CrossRef](#)]
77. Ngo, N.M.; Nguyen, M.N.; Song, S.-W.; Park, S. Bimetallic metal organic Framework-modified glass fiber as composite separator for lithium sulfur batteries. *Mater. Lett.* **2025**, *382*, 137835. [[CrossRef](#)]
78. Wild, M.; O'Neill, L.; Zhang, T.; Purkayastha, R.; Minton, G.; Marinescu, M.; Offer, G.J. Lithium sulfur batteries, a mechanistic review. *Energy Environ. Sci.* **2015**, *8*, 3477–3494. [[CrossRef](#)]
79. Wu, L.; Yuan, C.; Gao, F.; Qiang, X.; Hui, J.; Liu, B. Self-assembly of polyoxometalate-based metal-organic framework with trefoil sign structural feature as efficient anode for lithium ion batteries. *Solid State Sci.* **2025**, *159*, 107774. [[CrossRef](#)]
80. Ren, W.; Ma, W.; Zhang, S.; Tang, B. Recent advances in shuttle effect inhibition for lithium sulfur batteries. *Energy Storage Mater.* **2019**, *23*, 707–732. [[CrossRef](#)]
81. Deng, W.; Phung, J.; Li, G.; Wang, X. Realizing high-performance lithium-sulfur batteries via rational design and engineering strategies. *Nano Energy* **2021**, *82*, 105761. [[CrossRef](#)]
82. Liu, T.; Hu, H.; Ding, X.; Yuan, H.; Jin, C.; Nai, J.; Liu, Y.; Wang, Y.; Wan, Y.; Tao, X. 12 years roadmap of the sulfur cathode for lithium sulfur batteries (2009–2020). *Energy Storage Mater.* **2020**, *30*, 346–366. [[CrossRef](#)]
83. Eftekhari, A.; Kim, D.-W. Cathode materials for lithium-sulfur batteries: A practical perspective. *J. Mater. Chem.* **2017**, *5*, 17734–17776. [[CrossRef](#)]
84. Demir-Cakan, R.; Morcrette, M.; Nouar, F.; Davoisne, C.; Devic, T.; Gonbeau, D.; Dominko, R.; Serre, C.; Ferey, G.; Tarascon, J.M. Cathode composites for Li-S batteries via the use of oxygenated porous architectures. *J. Am. Chem. Soc.* **2011**, *133*, 16154–16160. [[CrossRef](#)] [[PubMed](#)]
85. Hou, Y.; Mao, H.; Xu, L. MIL-100(V) and MIL-100(V)/rGO with various valence states of vanadium ions as sulfur cathode hosts for lithium-sulfur batteries. *Nano Res.* **2016**, *10*, 344–353. [[CrossRef](#)]
86. Hong, X.J.; Tan, T.X.; Guo, Y.K.; Tang, X.Y.; Wang, J.Y.; Qin, W.; Cai, Y.P. Confinement of polysulfides within bi-functional metal-organic frameworks for high performance lithium-sulfur batteries. *Nanoscale* **2018**, *10*, 2774–2780. [[CrossRef](#)]
87. Wang, Z.; Li, X.; Cui, Y.; Yang, Y.; Pan, H.; Wang, Z.; Wu, C.; Chen, B.; Qian, G. A metal-organic framework with open metal sites for enhanced confinement of sulfur and lithium-sulfur battery of long cycling life. *Cryst. Growth Des.* **2013**, *13*, 5116–5120. [[CrossRef](#)]
88. Haro, J.; Benítez, A.; Caballero, Á.; Morales, J. Revisiting the HKUST-1/S composite as an electrode for Li-S batteries: Inherent problems that hinder its performance. *Eur. J. Inorg. Chem.* **2020**, *2021*, 177–185. [[CrossRef](#)]
89. Feng, Y.; Zhang, Y.; Du, G.; Zhang, J.; Liu, M.; Qu, X. Li₂S-Embedded copper metal-organic framework cathode with superior electrochemical performance for Li-S batteries. *New J. Chem.* **2018**, *42*, 13775–13783. [[CrossRef](#)]
90. Feng, Y.; Zhang, Y.; Du, G.; Zhang, J.; Qu, X. Experimental and first-principles study of a metal-organic framework with sulfur embedding cathode for enhanced performance lithium-sulfur battery. *Sustain. Energy Fuels* **2018**, *2*, 1828–1836. [[CrossRef](#)]
91. Zhou, J.; Yu, X.; Fan, X.; Wang, X.; Li, H.; Zhang, Y.; Li, W.; Zheng, J.; Wang, B.; Li, X. The impact of the particle size of a metal-organic framework for sulfur storage in Li-S batteries. *J. Mater. Chem.* **2015**, *3*, 8272–8275. [[CrossRef](#)]
92. Cui, G.; Li, G.; Luo, D.; Zhang, Y.; Zhao, Y.; Wang, D.; Wang, J.; Zhang, Z.; Wang, X.; Chen, Z. Three-dimensionally ordered macromicroporous metal organic frameworks with strong sulfur immobilization and catalyzation for high-performance lithium-sulfur batteries. *Nano Energy* **2020**, *72*, 104685. [[CrossRef](#)]
93. Liu, Q.; Wang, R.; Liu, Z.; Wang, X.; Han, C.; Liu, H.; Li, B. A 3D lithiophilic ZIF-8@RGO free-standing scaffold with dendrite-free behavior enabling high performance Li metal batteries. *J. Mater. Chem. A* **2023**, *11*, 12910. [[CrossRef](#)]
94. Bai, L.; Chao, D.; Xing, P.; Tou, L.J.; Chen, Z.; Jana, A.; Shen, Z.X.; Zhao, Y. Refined sulfur nanoparticles immobilized in metal-organic polyhedron as stable cathodes for Li-S battery. *ACS Appl. Mater. Interfaces* **2016**, *8*, 14328–14333. [[CrossRef](#)] [[PubMed](#)]
95. Ge, X.; Li, C.; Li, Z.; Yin, L. Tannic acid tuned metal-organic framework as a high-efficiency chemical anchor of polysulfide for lithium-sulfur batteries. *Electrochim. Acta* **2018**, *281*, 700–709. [[CrossRef](#)]
96. Wu, Z.; Wang, L.; Chen, S.; Zhu, X.; Deng, Q.; Wang, J.; Zeng, Z.; Deng, S. Facile and low-temperature strategy to prepare hollow ZIF-8/CNT polyhedrons as high-performance lithium-sulfur cathodes. *Chem. Eng. J.* **2021**, *404*, 126579. [[CrossRef](#)]
97. Kaye, S.S.; Dailly, A.; Yaghi, O.M.; Long, J.R. Impact of preparation and handling on the hydrogen storage properties of Zn₄O(1,4-benzenedicarboxylate)₃ (MOF-5). *J. Am. Chem. Soc.* **2007**, *129*, 14176–14177. [[CrossRef](#)]

98. Shanthi, P.M.; Hanumantha, P.J.; Gattu, B.; Sweeney, M.; Datta, M.K.; Kumta, P.N. Understanding the origin of irreversible capacity loss in non-carbonized carbonate-Based metal organic framework (MOF) sulfur hosts for lithium—Sulfur battery. *Electrochim. Acta* **2017**, *229*, 208–218. [CrossRef]
99. Wang, Z.; Wang, B.; Yang, Y.; Cui, Y.; Wang, Z.; Chen, B.; Qian, G. Mixed-metal-organic framework with effective Lewis acidic sites for sulfur confinement in high-performance lithium-sulfur batteries. *ACS Appl. Mater. Interfaces* **2015**, *7*, 20999–21004. [CrossRef]
100. Liu, B.; Baumann, A.E.; Thoi, V.S. Modulating charge transport in MOFs with zirconium oxide nodes and redox-active linkers for lithium sulfur batteries. *Polyhedron* **2019**, *170*, 788–795. [CrossRef]
101. Lai, M.; Zhang, D.; Chen, F.; Lin, X.; Qiu, A.; Lei, C.; Liang, J.; Liang, J.; Li, J.; Wang, Q.; et al. Advanced Metal-Organic Frameworks Based on Anthraquinone-2,3-Dicarboxylate Ligands as Cathode for Lithium-Ion Batteries. *Batteries* **2023**, *9*, 247. [CrossRef]
102. Zhu, M.; Cai, C.; Quan, K.; Wei, Y.; Chen, H.; Zhang, S.; Yi, H.; Guo, Z.; Teng, X.; Zhang, J. Two-dimensional metal-organic frameworks with highly exposed active centers as a synergistic protective interlayer for shuttle-free lithium-sulfur batteries. *Chem. Eng. Sci.* **2025**, *306*, 121325. [CrossRef]
103. Park, B. Pseudocapacitive charge storage in ultrathin NiCo-metal organic framework-derived NiCo₂O₄ Li-metal batteries. *Mater. Lett.* **2025**, *394*, 138654. [CrossRef]
104. Yang, T.; Xiao, R.; Lu, F.; Ke, X.; Wang, M.; Wang, K. Conductivity enhancement mechanism and application of NiCo-MOF hollow sphere electrode materials in lithium-ion batteries. *New J. Chem.* **2025**, *49*, 6674–6683. [CrossRef]
105. Wei, H.; Qin, F. Electrochemical Synthesis and Conductivity Fine Tuning of the 2D Iron-Quinoid Metal-Organic Framework. *ACS Appl. Mater. Interfaces* **2025**, *17*, 2010–2017. [CrossRef]
106. Zanca, F.; Glasby, L.T.; Chong, S.; Chen, S.; Kim, J.; Fairen-Jimenez, D.; Monserrat, B.; Moghadam, P.Z. Computational techniques for characterisation of electrically conductive MOFs: Quantum calculations and machine learning approaches. *J. Mater. Chem. C* **2021**, *9*, 13584–13599. [CrossRef]
107. Zhang, J.; Liu, Y.; Wang, T.; Fu, N.; Yang, Z. Manganese-based MOF interconnected carbon nanotubes as a high-performance cathode for rechargeable aqueous zinc-ion batteries. *J. Energy Storage* **2024**, *76*, 109873. [CrossRef]
108. Li, X.; Cheng, F.; Zhang, S.; Chen, J. Shape-controlled synthesis and lithium-storage study of metal-organic frameworks Zn₄O(1,3,5-benzenetribenzoate)₂. *J. Power Sources* **2006**, *160*, 542–547. [CrossRef]
109. de Combarieu, G.; Morcrette, M.; Millange, F.; Guillou, N.; Cabana, J.; Grey, C.P.; Margiolaki, I.; Férey, G.; Tarascon, J.M. Influence of the benzoquinone sorption on the structure and electrochemical performance of the MIL-53(Fe) hybrid porous material in a lithium-ion battery. *Chem. Mater.* **2009**, *21*, 1602–1611. [CrossRef]
110. Fateeva, A.; Horcajada, P.; Devic, T.; Serre, C.; Marrot, J.; Grenèche, J.-M.; Morcrette, M.; Tarascon, J.-M.; Maurin, G.; Férey, G. Synthesis, structure, characterization, and redox properties of the porous MIL-68(Fe) solid. *Eur. J. Inorg. Chem.* **2010**, *2010*, 3789–3794. [CrossRef]
111. Shin, J.; Kim, M.; Cirera, J.; Chen, S.; Halder, G.J.; Yersak, T.A.; Paesani, F.; Cohen, S.M.; Meng, Y.S. MIL-101(Fe) as a lithium-ion battery electrode material: A relaxation and intercalation mechanism during lithium insertion. *J. Mater. Chem.* **2015**, *3*, 4738–4744. [CrossRef]
112. Deng, S.-Q.; Zhuang, Z.; Zhou, C.-A.; Zheng, H.; Zheng, S.-R.; Yan, W.; Zhang, J. Metal-organic framework derived FeNi alloy nanoparticles embedded in N-doped porous carbon as high-performance bifunctional air-cathode catalysts for rechargeable zinc-air battery. *J. Colloid Interface Sci.* **2023**, *641*, 265–276. [CrossRef]
113. Li, C.; Zhang, C.; Xie, J.; Wang, K.; Li, J.; Zhang, Q. Ferrocene-based metal-organic framework as a promising cathode in lithium-ion battery. *Chem. Eng. J.* **2021**, *404*, 126463. [CrossRef]
114. Chen, T.; Wang, F.; Cao, S.; Bai, Y.; Zheng, S.; Li, W.; Zhang, S.; Hu, S.X.; Pang, H. In situ synthesis of MOF-74 family for high areal energy density of aqueous nickel-zinc batteries. *Adv. Mater.* **2022**, *34*, e2201779. [CrossRef]
115. Li, Z.; Wang, Y.; Zhao, F.; Li, Y.; Yan, H.; Xu, B.; Sun, D. Moss-like two-dimensional MBene-Ni/Co bimetallic metal-organic framework composite as efficient cathode for alkaline zinc batteries. *J. Power Sources* **2025**, *633*, 236437. [CrossRef]
116. Peng, Z.; Yi, X.; Liu, Z.; Shang, J.; Wang, D. Triphenylamine-based metal-organic frameworks as cathode materials in lithium-ion batteries with coexistence of redox active sites, high working voltage, and high rate stability. *ACS Appl. Mater. Interfaces* **2016**, *8*, 14578–14585. [CrossRef] [PubMed]
117. Nagatomi, H.; Yanai, N.; Yamada, T.; Shiraishi, K.; Kimizuka, N. Synthesis and electric properties of a two-dimensional metal-organic framework based on phthalocyanine. *Chemistry* **2018**, *24*, 1806–1810. [CrossRef]
118. Gu, S.; Bai, Z.; Majumder, S.; Huang, B.; Chen, G. Conductive metal-organic framework with redox metal center as cathode for high rate performance lithium ion battery. *J. Power Sources* **2019**, *429*, 22–29. [CrossRef]
119. Spinner, N.; Zhang, L.; Mustain, W.E. Investigation of metal oxide anode degradation in lithium-ion batteries via identical-location TEM. *J. Mater. Chem. A* **2014**, *2*, 1627. [CrossRef]
120. Xia, F.; Zeng, W.; Peng, H.; Wang, H.; Sun, C.; Zou, J.; Wu, J. Revealing structural degradation in layered structure oxides cathode of lithium ion batteries via in-situ transmission electron microscopy. *J. Mater. Sci. Technol.* **2023**, *154*, 189–201. [CrossRef]

121. Tian, B.; Ning, G.H.; Gao, Q.; Tan, L.M.; Tang, W.; Chen, Z.; Su, C.; Loh, K.P. Crystal engineering of naphthalenediimide-based metal-organic frameworks: Structure-dependent lithium storage. *ACS Appl. Mater. Interfaces* **2016**, *8*, 31067–31075. [CrossRef]
122. Bi, D.; Zhao, T.; Lai, Q.; Zhao, J.; Grigoriev, S.A.; Liang, Y.Y. In situ preparation of MOF-74 for compact zincophilic surfaces enhancing the stability of aqueous zinc-ion battery anodes. *J. Alloys Compd.* **2024**, *1002*, 175448. [CrossRef]
123. Qiao, Q.-Q.; Li, G.-R.; Wang, Y.-L.; Gao, X.-P. To enhance the capacity of Li-rich layered oxides by surface modification with metal-organic frameworks (MOFs) as cathodes for advanced lithium-ion batteries. *J. Mater. Chem.* **2016**, *4*, 4440–4447. [CrossRef]
124. Xu, Y.; Li, X.; Wang, X.; Weng, Q.; Sun, W. Engineering the conductive network of missing-linker metal-organic framework for improved performance in aqueous zinc-ion batteries. *J. Power Sources* **2024**, *624*, 235525. [CrossRef]
125. Yu, T.; Cai, R.; Chen, Z. Zn-air batteries. In *Metal-Air Batteries: Fundamentals and Applications*; Zhang, X.-B., Ed.; Wiley-VCH: Hoboken, NJ, USA, 2018; pp. 265–291, ISBN 978-3-527-80766-6.
126. Gilligan, G.E.; Qu, D. Zinc-air and other types of metal-air batteries. In *Advances in Batteries for Medium and Large-Scale Energy Storage*; Menictas, C., Skyllas-Kazacos, M., Lim, T.M., Eds.; Woodhead Publishing: Sawston, UK, 2015; pp. 441–461. [CrossRef]
127. Li, H.; Ma, L.; Han, C.; Wang, Z.; Liu, Z.; Tang, Z.; Zhi, C. Advanced rechargeable zinc-based batteries: Recent progress and future perspectives. *Nano Energy* **2019**, *62*, 550–587. [CrossRef]
128. Zhang, W.; Liu, Y.; Zhang, L.; Chen, J. Recent advances in isolated single-atom catalysts for zinc air batteries: A focus review. *Nanomaterials* **2019**, *9*, 1402. [CrossRef] [PubMed]
129. He, Y.; Aasen, D.; Yu, H.; Labbe, M.; Ivey, D.G.; Veinot, J.G.C. Mn₃O₄ nanoparticle-decorated hollow mesoporous carbon spheres as an efficient catalyst for oxygen reduction reaction in Zn-air batteries. *Nanoscale Adv.* **2020**, *2*, 3367–3374. [CrossRef]
130. Gu, Y.; Yan, G.; Lian, Y.; Qi, P.; Mu, Q.; Zhang, C.; Deng, Z.; Peng, Y. MnIII-enriched a-MnO₂ nanowires as efficient bifunctional oxygen catalysts for rechargeable Zn-air batteries. *Energy Storage Mater.* **2019**, *23*, 252–260. [CrossRef]
131. Yan, W.; Guo, Z.; Xu, H.; Lou, Y.; Chen, J.; Li, Q. Downsizing metal-organic frameworks with distinct morphologies as cathode materials for high-capacity Li₂O₂ batteries. *Mater. Chem. Front.* **2017**, *1*, 1324–1330. [CrossRef]
132. Lv, C.; Li, B.; Ren, Y.; Zhang, G.; Lu, Z.; Li, L.; Zhang, X.; Yang, X.; Yu, X. A “MOF-plus-MOF” strategy to synthesize Co-N3C1 single-atom catalyst for rechargeable Zn-air battery. *Chem. Eng. J.* **2024**, *495*, 153670. [CrossRef]
133. Kim, S.H.; Lee, Y.J.; Kim, D.H.; Lee, Y.J. Bimetallic metal-organic frameworks as efficient cathode catalysts for Li-O₂ batteries. *ACS Appl. Mater. Interfaces* **2018**, *10*, 660–667. [CrossRef]
134. Hu, X.; Zhu, Z.; Cheng, F.; Tao, Z.; Chen, J. Micro-nano structured Ni-MOFs as high-performance cathode catalyst for rechargeable Li-O₂ batteries. *Nanoscale* **2015**, *7*, 11833–11840. [CrossRef]
135. Wang, Y.; Tao, L.; Xiao, Z.; Chen, R.; Jiang, Z.; Wang, S. 3D carbon electrocatalysts in situ constructed by defect-rich nanosheets and polyhedrons from NaCl-sealed zeolitic imidazolate frameworks. *Adv. Funct. Mater.* **2018**, *28*, 1705356. [CrossRef]
136. Yang, M.; Hu, X.; Fang, Z.; Sun, L.; Yuan, Z.; Wang, S.; Hong, W.; Chen, X.; Yu, D. Bifunctional MOF-derived carbon photonic crystal architectures for advanced Zn-air and Li-S batteries: Highly exposed graphitic nitrogen matters. *Adv. Funct. Mater.* **2017**, *27*, 1701971. [CrossRef]
137. Liu, Z.; Liu, J.; Wu, H.B.; Shen, G.; Le, Z.; Chen, G.; Lu, Y. Iron-decorated nitrogen-rich carbons as efficient oxygen reduction electrocatalysts for Zn-air batteries. *Nanoscale* **2018**, *10*, 16996–17001. [CrossRef] [PubMed]
138. Zhang, X.; Han, X.; Jiang, Z.; Xu, J.; Chen, L.; Xue, Y.; Nie, A.; Xie, Z.; Kuang, Q.; Zheng, L. Atomically dispersed hierarchically ordered porous Fe-N-C electrocatalyst for high performance electrocatalytic oxygen reduction in Zn-Air battery. *Nano Energy* **2020**, *71*, 104547. [CrossRef]
139. Zhang, Z.; Jin, H.; Zhu, J.; Li, W.; Zhang, C.; Zhao, J.; Luo, F.; Sun, Z.; Mu, S. 3D flower-like ZnFe-ZIF derived hierarchical Fe, N-Codoped carbon architecture for enhanced oxygen reduction in both alkaline and acidic media, and zinc-air battery performance. *Carbon* **2020**, *161*, 502–509. [CrossRef]
140. Jin, H.; Zhou, H.; Li, W.; Wang, Z.; Yang, J.; Xiong, Y.; He, D.; Chen, L.; Mu, S. In situ derived Fe/N/S-codoped carbon nanotubes from ZIF-8 crystals as efficient electrocatalysts for the oxygen reduction reaction and zinc-air batteries. *J. Mater. Chem.* **2018**, *6*, 20093–20099. [CrossRef]
141. Chen, K.; Ci, S.; Xu, Q.; Cai, P.; Li, M.; Xiang, L.; Hu, X.; Wen, Z. Iron-incorporated nitrogen-doped carbon materials as oxygen reduction electrocatalysts for zinc-air batteries. *Chin. J. Catal.* **2020**, *41*, 858–867. [CrossRef]
142. Chen, D.; Ji, J.; Jiang, Z.; Ling, M.; Jiang, Z.; Peng, X. Molecular-confinement synthesis of sub-nano Fe/N/C catalysts with high oxygen reduction reaction activity and excellent durability for rechargeable Zn-Air batteries. *J. Power Sources* **2020**, *450*, 227660. [CrossRef]
143. Li, J.-C.; Wu, X.-T.; Chen, L.-J.; Li, N.; Liu, Z.-Q. Bifunctional MOF-derived Co-N-doped carbon electro-catalysts for high-performance zinc-air batteries and MFCs. *Energy* **2018**, *156*, 95–102. [CrossRef]
144. Amiinu, I.S.; Liu, X.; Pu, Z.; Li, W.; Li, Q.; Zhang, J.; Tang, H.; Zhang, H.; Mu, S. From 3D ZIF nanocrystals to Co-N_x/C nanorod array electrocatalysts for ORR, OER, and Zn-air batteries. *Adv. Funct. Mater.* **2018**, *28*, 1704638. [CrossRef]
145. Zhang, M.; Dai, Q.; Zheng, H.; Chen, M.; Dai, L. Novel MOF-derived Co@N-C bifunctional catalysts for highly efficient Zn-air batteries and water splitting. *Adv. Mater.* **2018**, *30*, 1705431. [CrossRef] [PubMed]

146. Zang, W.; Sumboja, A.; Ma, Y.; Zhang, H.; Wu, Y.; Wu, S.; Wu, H.; Liu, Z.; Guan, C.; Wang, J.; et al. Single Co atoms anchored in porous N-doped carbon for efficient zinc-air battery cathodes. *ACS Catal.* **2018**, *8*, 8961–8969. [[CrossRef](#)]
147. Zhang, X.; Luo, J.; Lin, H.-F.; Tang, P.; Morante, J.R.; Arbiol, J.; Wan, K.; Mao, B.-W.; Liu, L.-M.; Fransaer, J. Tailor-made metal-nitrogen-carbon bifunctional electrocatalysts for rechargeable Zn-air batteries via controllable MOF units. *Energy Storage Mater.* **2019**, *17*, 46–61. [[CrossRef](#)]
148. Zhong, B.; Zhang, L.; Yu, J.; Fan, K. Ultrafine iron-cobalt nanoparticles embedded in nitrogen-doped porous carbon matrix for oxygen reduction reaction and zinc-air batteries. *J. Colloid Interface Sci.* **2019**, *546*, 113–121. [[CrossRef](#)]
149. Duan, X.; Ren, S.; Pan, N.; Zhang, M.; Zheng, H. MOF-derived Fe₃Co₄@NeC bifunctional oxygen electro-catalysts for Zn-air batteries. *J. Mater. Chem.* **2020**, *8*, 9355–9363. [[CrossRef](#)]
150. Shin, S.; Yoon, H.; Yoon, Y.; Park, S.; Shin, M.W. Porosity tailoring of the Zn-MOF-5 derived carbon materials and its effects on the performance as a cathode for lithium-air batteries. *Microporous Mesoporous Mater.* **2021**, *311*, 110726. [[CrossRef](#)]
151. Ge, Q.; Chen, M.; Lou, X.; Zhang, W.; Shen, M.; Yang, Q.; Hu, B. Centrifugal field guided dual templating synthesis of functional macro-microporous carbon. *Part. Part. Syst. Char.* **2018**, *35*, 1800262. [[CrossRef](#)]
152. Yu, H.; Dinh, K.N.; Sun, Y.; Fan, H.; Wang, Y.; Jing, Y.; Li, S.; Srinivasan, M.; Yan, Q. Performance-improved Li-O₂ batteries by tailoring the phases of Mo_xC porous nanorods as an efficient cathode. *Nanoscale* **2018**, *10*, 14877–14884. [[CrossRef](#)]
153. Wang, Q.; Wang, X.; He, H. Integrated 3D foam-like porous Ni₃S₂ as improved deposition support for high-performance Li₂O₂ battery. *J. Power Sources* **2020**, *448*, 227397. [[CrossRef](#)]
154. Zhang, P.; Hui, X.; Wang, H.; Gao, X.; Yin, L. Porous hollow ZnCo₂S₄ nanosheet arrays derived from metal-organic framework as efficient cathode for lithium oxygen batteries. *J. Alloys Compd.* **2021**, *860*, 157656. [[CrossRef](#)]
155. Zhang, H.; Zhao, W.Q.; Zou, M.C.; Wang, Y.S.; Chen, Y.J.; Xu, L.; Wu, H.S.; Cao, A.Y. 3D, mutually embedded MOF@carbon nanotube hybrid networks for high-performance lithium-sulfur batteries. *Adv. Energy Mater.* **2018**, *8*, 1800013. [[CrossRef](#)]
156. Ji, X.; Li, Q.; Yu, H.; Hu, X.; Luo, Y.; Li, B. Three-dimensional ordered macroporous ZIF-8 nanoparticle-derived nitrogen-doped hierarchical porous carbons for high-performance lithium-sulfur batteries. *RSC Adv.* **2020**, *10*, 41983–41992. [[CrossRef](#)] [[PubMed](#)]
157. Zhang, J.; Huang, M.; Xi, B.; Mi, K.; Yuan, A.; Xiong, S. Systematic study of effect on enhancing specific capacity and electrochemical behaviors of lithium-sulfur batteries. *Adv. Energy Mater.* **2018**, *8*, 1701330. [[CrossRef](#)]
158. Li, Z.; Yin, L. Nitrogen-doped MOF-derived micropores carbon as immobilizer for small sulfur molecules as a cathode for lithium sulfur batteries with excellent electrochemical performance. *ACS Appl. Mater. Interfaces* **2015**, *7*, 4029–4038. [[CrossRef](#)] [[PubMed](#)]
159. Jiang, Y.; Liu, H.; Tan, X.; Guo, L.; Zhang, J.; Liu, S.; Guo, Y.; Zhang, J.; Wang, H.; Chu, W. Monoclinic ZIF-8 nanosheet-derived 2D carbon nanosheets as sulfur immobilizer for high-performance lithium sulfur batteries. *ACS Appl. Mater. Interfaces* **2017**, *9*, 25239–25249. [[CrossRef](#)]
160. Hao, G.P.; Tang, C.; Zhang, E.; Zhai, P.; Yin, J.; Zhu, W.; Zhang, Q.; Kaskel, S. Thermal exfoliation of layered metal-organic frameworks into ultrahydrophilic graphene stacks and their applications in Li-S batteries. *Adv. Mater.* **2017**, *29*, 1702829. [[CrossRef](#)]
161. Kim, D.; Kim, G.; Oh, S.; Park, J.; Lee, S.; Yoon, S.; Lee, J.; Lee, W.; Jeon, T.-Y.; Cho, E.; et al. Dual-doping of sulfur on mesoporous carbon as a cathode for the oxygen reduction reaction and lithium-sulfur batteries. *ACS Sustain. Chem. Eng.* **2020**, *8*, 8537–8548. [[CrossRef](#)]
162. Liu, Y.; Si, L.; Zhou, X.; Liu, X.; Xu, Y.; Bao, J.; Dai, Z. A selenium-confined microporous carbon cathode for ultrastable lithium-selenium batteries. *J. Mater. Chem. A* **2014**, *2*, 17735–17739. [[CrossRef](#)]
163. Li, Z.; Yin, L. MOF-derived, N-doped, hierarchically porous carbon sponges as immobilizers to confine selenium as cathodes for Li-Se batteries with superior storage capacity and perfect cycling stability. *Nanoscale* **2015**, *7*, 9597–9606. [[CrossRef](#)]
164. Jin, W.-W.; Li, H.-J.; Zou, J.-Z.; Inguva, S.; Zhang, Q.; Zeng, S.-Z.; Xu, G.-Z.; Zeng, X.-R. Metal organic framework-derived carbon nanosheets with fish-scale surface morphology as cathode materials for lithium-selenium batteries. *J. Alloys Compd.* **2020**, *820*, 153084. [[CrossRef](#)]
165. Yin, C.; Zhou, H.; Yang, Z.; Li, J. Synthesis and electrochemical properties of LiNi_{0.5}Mn_{1.5}O₄ for Li-ion batteries by the metal-organic framework method. *ACS Appl. Mater. Interfaces* **2018**, *10*, 13625–13634. [[CrossRef](#)] [[PubMed](#)]
166. Ding, Y.; Peng, Y.; Chen, W.; Niu, Y.; Wu, S.; Zhang, X.; Hu, L. V-MOF derived porous V₂O₅ nanoplates for high performance aqueous zinc ion battery. *Appl. Surf. Sci.* **2019**, *493*, 368–374. [[CrossRef](#)]
167. Bates, A.M.; Preger, Y.; Torres-Castro, L.; Harrison, K.L.; Harris, S.J.; Hewson, J. Are solid-state batteries safer than lithium-ion batteries? *Joule* **2022**, *6*, 742–755. [[CrossRef](#)]
168. Ye, L.; Li, X. A dynamic stability design strategy for lithium metal solid state batteries. *Nature* **2021**, *593*, 218–222. [[CrossRef](#)]
169. Lou, S.; Zhang, F.; Fu, C.; Chen, M.; Ma, Y.; Yin, G.; Wang, J. Interface Issues and Challenges in All-Solid-State Batteries: Lithium, Sodium, and Beyond. *Adv. Mater.* **2021**, *33*, 2000721. [[CrossRef](#)]
170. Hatzell, K.B.; Chen, X.C.; Cobb, C.L.; Dasgupta, N.P.; Dixit, M.B.; Marbella, L.E.; McDowell, M.T.; Mukherjee, P.P.; Verma, A.; Viswanathan, V.; et al. Challenges in Lithium Metal Anodes for Solid-State Batteries. *ACS Energy Lett.* **2020**, *5*, 922–934. [[CrossRef](#)]

171. Wei, Y.; Zhou, H.; Deng, H.; Ji, W.; Tia, K.; Ma, Z.; Zhang, K.; Fu, Q. “Toolbox” for the Processing of Functional Polymer Composites. *Nano Micro Lett.* **2022**, *14*, 35. [[CrossRef](#)]
172. Lin, R.; Jin, Y.; Li, Y.; Zhang, X.; Xiong, Y. Recent Advances in Ionic Liquids—MOF Hybrid Electrolytes for Solid-State Electrolyte of Lithium Battery. *Batteries* **2023**, *9*, 314. [[CrossRef](#)]
173. Xu, L.; Xiao, X.; Tu, H.; Zhu, F.; Wang, J.; Liu, H.; Huang, W.; Deng, W.; Hou, H.; Liu, T.; et al. Engineering Functionalized 2D Metal–Organic Frameworks Nanosheets with Fast Li⁺ Conduction for Advanced Solid Li Batteries. *Adv. Mater.* **2023**, *35*, 2303193. [[CrossRef](#)]
174. Liu, C.; Fu, X.; Liao, S.; Zou, G.; Yang, H. Interface Engineering Enables High-Performance Sb Anode for Sodium Storage. *Nanomaterials* **2023**, *13*, 254. [[CrossRef](#)]
175. Deng, X.; Tian, Y.; Zou, K.; Chen, J.; Xiao, X.; Tao, S.; Song, Z.; Deng, W.; Hou, H.; Zou, G.; et al. K_xC_y phase induced expanded interlayer in ultra-thin carbon toward full potassium-ion capacitors. *Carbon Energy* **2022**, *4*, 1151. [[CrossRef](#)]
176. Wu, J.-F.; Guo, X. Nanostructured Metal–Organic Framework (MOF)-Derived Solid Electrolytes Realizing Fast Lithium Ion Transportation Kinetics in Solid-State Batteries. *Small* **2019**, *15*, 1804413. [[CrossRef](#)] [[PubMed](#)]
177. Wang, Z.; Tan, R.; Wang, H.; Yang, L.; Hu, J.; Chen, H.; Pan, F. A Metal–Organic-Framework-Based Electrolyte with Nanowetted Interfaces for High-Energy-Density Solid-State Lithium Battery. *Adv. Mater.* **2018**, *30*, 1704436. [[CrossRef](#)]
178. Wang, Z.; Zhou, H.; Meng, C.; Xiong, W.; Cai, Y.; Hu, P.; Pang, H.; Yuan, A. Enhancing Ion Transport: Function of Ionic Liquid Decorated MOFs in Polymer Electrolytes for All-Solid-State Lithium Batteries. *ACS Appl. Energy Mater.* **2020**, *3*, 4265–4274. [[CrossRef](#)]
179. Yu, J.; Guo, T.; Wang, C.; Shen, Z.; Dong, X.; Li, S.; Zhang, H.; Lu, Z. Engineering Two-Dimensional Metal–Organic Framework on Molecular Basis for Fast Li⁺ Conduction. *Nano Lett.* **2021**, *21*, 5805–5812. [[CrossRef](#)]
180. Pettinari, C.; Tombesi, A. MOFs for electrochemical energy conversion and storage. *Inorganics* **2023**, *11*, 65. [[CrossRef](#)]
181. Vielstich, W.; Lamm, A.; Gasteiger, H.A. (Eds.) *Handbook of Fuel Cells*; John Wiley and Sons: New York, NY, USA, 2009; ISBN 978-0-470-74151-1.
182. Wong, C.Y.; Wong, W.Y.; Sudarsono, W.; Loh, K.S.; Lim, K.L.; Bo, W. Tuning the functionality of metal–organic frameworks (MOFs) for fuel cells and hydrogen storage applications. *J. Mater. Sci.* **2023**, *58*, 8637–8677. [[CrossRef](#)]
183. Sudarsono, W.; Tan, S.Y.; Wong, W.Y.; Omar, F.S.; Ramya, K.; Mehmood, S.; Numan, A.; Walvekar, R.; Khalid, M. From catalyst structure design to electrode fabrication of platinum-free electrocatalysts in proton exchange membrane fuel cells: A review. *J. Ind. Eng. Chem.* **2023**, *122*, 1–26. [[CrossRef](#)]
184. Chen, Z.; Kirlikovali, K.O.; Idrees, K.B.; Wasson, M.C.; Farha, O.K. Porous materials for hydrogen storage. *Chem* **2022**, *8*, 693–716. [[CrossRef](#)]
185. Jiao, L.; Jiang, H.-L. Metal–organic-framework-based single-atom catalysts for energy applications. *Chem* **2019**, *5*, 786–804. [[CrossRef](#)]
186. Tang, J.; Yamauchi, Y. Carbon materials: MOF morphologies in control. *Nat. Chem.* **2016**, *8*, 638–639. [[CrossRef](#)] [[PubMed](#)]
187. Wong, W.Y.; Rani, M.A.A.A.; Loh, K.S.; Lim, K.L.; Jeffery Minggu, L. Current progress on rational design of porous MOF-derived transition metal–nitrogen–carbon as oxygen reduction reaction catalysts for proton exchange membrane fuel cells. *Curr. Opin. Green. Sustain. Chem.* **2025**, *52*, 101001. [[CrossRef](#)]
188. Choi, I.; Lim, J.; dos Reis, R.; Kim, E.; Lim, S.Y.; Dravid, V.P.; Kim, H.; Oh, K.-H.; Nam, K.W. Metal–organic framework for high-performance catalyst layers in proton-exchange membrane fuel cells. *J. Mater. Chem. A* **2023**, *11*, 20583. [[CrossRef](#)]
189. Yin, R.; Ma, S.; Ying, J.; Lu, Z.; Niu, X.; Feng, J.; Xu, F.; Zheng, Y.; Liu, W.; Cao, X. MOF-Derived N-Doped C @ CoO/MoC Heterojunction Composite for Efficient Oxygen Reduction Reaction and Long-Life Zn–Air Battery. *Batteries* **2023**, *9*, 306. [[CrossRef](#)]
190. Dhanabalan, K.; Perumalsamy, M.; Sriram, G.; Murugan, N.; Shalu; Sadhasivam, T.; Oh, T.H. Metal–Organic Framework (MOF)-Derived Catalyst for Oxygen Reduction Reaction (ORR) Applications in Fuel Cell Systems: A Review of Current Advancements and Perspectives. *Energies* **2023**, *16*, 4950. [[CrossRef](#)]
191. Lu, X.F.; Fang, Y.; Luan, D.; Lou, X.W.D. Metal–organic frameworks derived functional materials for electrochemical energy storage and conversion: A mini review. *Nano Lett.* **2021**, *21*, 1555–1565. [[CrossRef](#)]
192. Radwan, A.; Jin, H.; He, D.; Mu, S. Design engineering, synthesis protocols, and energy applications of MOF-derived electrocatalysts. *Nano-Micro Lett.* **2021**, *13*, 132. [[CrossRef](#)]
193. Li, L.; He, J.; Wang, Y.; Lv, X.; Gu, X.; Dai, P.; Liu, D.; Zhao, X. Metal–organic frameworks: A promising platform for constructing non-noble electro-catalysts for the oxygen-reduction reaction. *J. Mater. Chem. A* **2019**, *7*, 1964–1988. [[CrossRef](#)]
194. Kang, I.; Lee, S.; Choi, W.-J.; Lee, S.; So, S.; Yu, D.M.; Yoon, S.J.; Kim, D.-W.; Nam, K.W.; Oh, K.-W. Effect of metal–organic framework on hydrogen volume fraction in the oxygen-rich anode catalyst layer of proton exchange membrane water electrolyzer. *Chem. Eng. J.* **2025**, *508*, 161094. [[CrossRef](#)]
195. Yu, S.; Jing, G.; Li, S.; Li, Z.; Ju, X. Tuning the hydrogen storage properties of MOF-650: A combined DFT and GCMC simulations study. *Int. J. Hydrogen Energy* **2020**, *45*, 6757–6764. [[CrossRef](#)]

196. Sule, R.; Mishra, A.K.; Nkambule, T.T. Recent advancement in consolidation of MOFs as absorbents for hydrogen storage. *Int. J. Energy Res.* **2021**, *45*, 12481–12499. [[CrossRef](#)]
197. Suresh, K.; Aulakh, D.; Purewal, J.; Siegel, D.J.; Veenstra, M.; Matzger, A.J. Optimizing hydrogen storage in MOFs through engineering of crystal morphology and control of crystal size. *J. Am. Chem. Soc.* **2021**, *143*, 10727–10734. [[CrossRef](#)] [[PubMed](#)]
198. Mahalingam, A.; Pushpara, H. Synthesis, Characterization, and Fabrication of Nickel Metal–Organic Framework-Incorporated Polymer Electrolyte Membranes for Fuel-Cell Applications. *ACS Appl. Mater. Interfaces* **2024**, *16*, 31145–31157. [[CrossRef](#)] [[PubMed](#)]
199. Lei, Z.; Shen, J.; Zhang, W.; Wang, Q.; Wang, J.; Deng, Y.; Wang, C. Exploring porous zeolitic imidazolate framework-8 (ZIF-8) as an efficient filler for high-performance poly(ethyleneoxide)-based solid polymer electrolytes. *Nano Res.* **2020**, *13*, 2259–2267. [[CrossRef](#)]
200. Zhu, B.; Sui, Y.; Wei, P.; Wen, J.; Cao, H.; Cong, C.; Meng, X.; Zhou, Q. NH₂-UiO-66 coated fibers to balance the excellent proton conduction efficiency and significant dimensional stability of proton exchange membrane. *J. Membr. Sci.* **2021**, *628*, 119214. [[CrossRef](#)]
201. Zhao, G.; Xu, X.; Zhao, H.; Shi, L.; Zhuang, X.; Cheng, B.; Yin, Y. Zeolitic imidazolate framework decorated on 3D nanofiber network towards superior proton conduction for proton exchange membrane. *J. Membr. Sci.* **2020**, *601*, 117914. [[CrossRef](#)]
202. Pathak, A.; Watanabe, H.; Manna, B.; Hatakeyama, K.; Ida, S. Hydrogen-Bonded Metal–Organic Framework Nanosheet as a Proton Conducting Membrane for an H₂/O₂ Fuel Cell. *Small* **2024**, *20*, 2400222. [[CrossRef](#)]
203. Li, Q.; Gao, W.; Zhang, N.; Gao, X.; Wu, D.; Che, Q. Preparation of high temperature proton exchange membranes with multilayered structures through alternate deposition of carbon dots@Metal organic framework and Sulfonated Poly(Ether Ketone). *J. Membr. Sci.* **2025**, *713*, 123306. [[CrossRef](#)]
204. Divya, K.; Liu, Q.; Murali, R.; Asghar, M.R.; Liu, H.; Zhang, W.; Xu, Q.; Ren, J.; Su, H. Integration of phosphorylated MOF/COF core-shell structures into hybrid membrane for high-temperature fuel cell application. *Appl. Surf. Sci.* **2025**, *681*, 161544. [[CrossRef](#)]
205. Ye, Y.; Gong, L.; Xiang, S.; Zhang, Z.; Chen, B. Metal-Organic Frameworks as a Versatile Platform for Proton Conductors. *Adv. Mater.* **2020**, *32*, e1907090. [[CrossRef](#)]
206. Du, J.; Yu, G.; Lin, H.; Jie, P.; Zhang, F.; Qu, F.; Wen, C.; Feng, L.; Liang, X. Enhanced proton conductivity of metal organic framework at low humidity by improvement in water retention. *J. Colloid. Interface Sci.* **2020**, *573*, 360–369. [[CrossRef](#)] [[PubMed](#)]
207. Ojha, R.; Pradhan, D. The potential of microbial fuel cell for converting waste to energy: An overview. *Sustain. Chem. Environ.* **2025**, *9*, 100196. [[CrossRef](#)]
208. Tremouli, A.; Kamperidis, T.; Pandis, P.K.; Argirasis, C.; Lyberatos, G. Exploitation of Digestate from Thermophilic and Mesophilic Anaerobic Digesters Fed with Fermentable Food Waste Using the MFC Technology. *Waste Biomass Valorization* **2021**, *12*, 5361–5370. [[CrossRef](#)]
209. Kamperidis, T.; Pandis, P.K.; Argirasis, C.; Lyberatos, G.; Tremouli, A. Effect of Food Waste Condensate Concentration on the Performance of Microbial Fuel Cells with Different Cathode Assemblies. *Sustainability* **2022**, *14*, 2625. [[CrossRef](#)]
210. Logan, B.E. Exoelectrogenic bacteria that power microbial fuel cells. *Nat. Rev. Microbiol.* **2009**, *7*, 375–381. [[CrossRef](#)]
211. Jiang, N.; Su, C.; Li, J.; Zhang, Y.; Wang, B.; Jiang, B.; Gao, W. Mesoporous silica-modified metal organic frameworks derived bimetallic electrocatalysts for oxygen reduction reaction in microbial fuel cells. *Int. J. Hydrogen Energy* **2025**, *97*, 571–580. [[CrossRef](#)]
212. Yoon, H.S.; Park, H.-Y.; Jung, W.S. Synergistic effects of fluorine and nitrogen dopants in fluorine/nitrogen-coordinated iron-co-doped carbon catalysts for enhanced oxygen reduction in alkaline media. *Int. J. Hydrogen Energy* **2024**, *60*, 1092–1100. [[CrossRef](#)]
213. Chu, C.; Liu, J.; Wei, L.; Feng, J.; Li, H.; Shen, J. Iron carbide and iron phosphide embedded N-doped porous carbon derived from biomass as oxygen reduction reaction catalyst for microbial fuel cell. *Int. J. Hydrogen Energy* **2023**, *48*, 4492–4502. [[CrossRef](#)]
214. Koo, B.; Jung, S.P. Improvement of air cathode performance in microbial fuel cells by using catalysts made by binding metal-organic framework and activated carbon through ultrasonication and solution precipitation. *Chem. Eng. J.* **2021**, *424*, 130388. [[CrossRef](#)]
215. Koo, B.; Lee, S.-M.; Oh, S.-E.; Kim, E.J.; Hwang, Y.; Seo, D.; Kim, J.Y.; Kahng, Y.H.; Lee, Y.W.; Chung, S.-Y.; et al. Addition of reduced graphene oxide to an activated-carbon cathode increases electrical power generation of a microbial fuel cell by enhancing cathodic performance. *Electrochim. Acta* **2018**, *297*, 613–622. [[CrossRef](#)]
216. Santoro, C.; Kodali, M.; Kabir, S.; Soavi, F.; Serov, A.; Atanassov, P. Three-dimensional graphene nanosheets as cathode catalysts in standard and supercapacitive microbial fuel cell. *J. Power Sources* **2017**, *356*, 371–380. [[CrossRef](#)] [[PubMed](#)]
217. Paul, S.; Choi, S.-J.; Kim, H.J. Enhanced Proton Conductivity of a Zn(II)-Based MOF/Aquivion Composite Membrane for PEMFC Applications. *Energy Fuels* **2020**, *34*, 10067–10077. [[CrossRef](#)]
218. Cao, J.; Su, C.; Ji, Y.; Yang, G.; Shao, Z. Recent advances and perspectives of fluorite and perovskite-based dual-ion conducting solid oxide fuel cells. *J. Energy Chem.* **2021**, *57*, 406–427. [[CrossRef](#)]

219. Wang, H.; Zhao, Y.; Shao, Z.; Xu, W.; Wu, Q.; Ding, X.; Hou, H. Proton conduction of Nafion hybrid membranes promoted by NH₃-modified Zn-MOF with host-guest collaborative hydrogen bonds for H₂/O₂ fuel cell applications. *ACS Appl. Mater. Interfaces* **2021**, *13*, 7485–7497. [CrossRef]
220. Yoo, D.K.; Lee, G.; Mondol, M.H.; Lee, H.J.; Kim, C.M.; Jhung, S.H. Preparation and applications of metal–organic frameworks composed of sulfonic acid. *Coord. Chem. Rev.* **2023**, *474*, 214868. [CrossRef]
221. Li, X.-M.; Gao, J. Recent advances of metal–organic frameworks-based proton exchange membranes in fuel cell applications. *SusMat.* **2022**, *2*, 504–534. [CrossRef]
222. Mukhopadhyay, S.; Das, A.; Jana, T.; Das, S.K. Fabricating a MOF Material with Polybenzimidazole into an Efficient Proton Exchange Membrane. *ACS Appl. Energy Mater.* **2020**, *3*, 7964–7977. [CrossRef]
223. Li, D.; Zhang, L.; Kuang, L.; Qin, H.; Hu, X.; He, J.; Ni, H.; He, Y. Carbothermal shock synthesis of CoO/N/C nanoparticles with superior durability for oxygen reduction reaction. *J. Power Sources* **2023**, *587*, 233699. [CrossRef]
224. Wang, Z.; Lu, Y.; Yan, Y.; Larissa, T.Y.P.; Zhang, X.; Wuu, D.; Zhang, H.; Yang, Y.; Wang, X. Core-shell carbon materials derived from metal-organic frameworks as an efficient oxygen bifunctional electrocatalyst. *Nano Energy* **2016**, *30*, 368–378. [CrossRef]
225. Zhang, L.; Zhang, L.; Li, D.; Qin, H.; Ni, H.; Chi, H.; He, J.; He, Y. Metal-organic framework derived Co@N/C with enhanced oxygen reduction reaction in direct borohydride fuel cells. *Chem. Eng. Sci.* **2025**, *303*, 120953. [CrossRef]
226. Parsa, S.M.; Chen, Z.; Feng, S.; Yang, Y.; Luo, L.; Ngo, H.H.; Wei, W.; Ni, B.-J.; Guo, W. Metal-free nitrogen-doped carbon-based electrocatalysts for oxygen reduction reaction in microbial fuel cells: Advances, challenges, and future directions. *Nano Energy* **2025**, *134*, 110537. [CrossRef]
227. Li, C.; Song, Z.; Liu, H. Octahedral copper metal-organic framework grafted with MoS₂ nanoflowers for high-performance oxygen reduction reaction. *J. Environ. Chem. Eng.* **2025**, *13*, 115856. [CrossRef]
228. Zhang, X.; Huang, G.; Lan, F.; Liu, Y.; Wang, R.; Yang, Y.; Chen, J. Boosting oxygen reduction in microbial fuel cells with zeolitic imidazolate frameworks-coated molybdenum disulfide as cathode catalyst. *J. Power Sources* **2025**, *632*, 236386. [CrossRef]
229. Zhu, L.; Han, T.; Ding, Y.; Long, J.; Lin, X.; Liu, J. A Metal-Organic-Framework Derived NiFe₂O₄@NiCo-LDH Nanocube as High-Performance Lithium-Ion Battery Anode Under Different Temperatures. *Appl. Surf. Sci.* **2022**, *599*, 153953. [CrossRef]
230. Wang, J.; Zhou, H.; Zhu, M.; Yuan, A.; Shen, X. Metal-organic framework-derived Co₃O₄ covered by MoS₂ nanosheets for high-performance lithium-ion batteries. *J. Alloys Compd.* **2018**, *744*, 220–227. [CrossRef]
231. Wang, Y.; Kong, M.; Liu, Z.; Lin, C.; Zeng, Y. Morella-rubra-like metal-organic-framework-derived multilayered Co₃O₄/NiO/C hybrids as high-performance anodes for lithium storage. *J. Mater. Chem. A* **2017**, *5*, 24269–24274. [CrossRef]
232. Peng, H.-J.; Hao, G.-X.; Chu, Z.-H.; Lin, Y.-W.; Lin, X.-M.; Cai, Y.-P. Porous carbon with large surface area derived from a metal-organic framework as a lithium-ion battery anode material. *RSC Adv.* **2017**, *7*, 34104–34109. [CrossRef]
233. Sun, C.; Yang, J.; Rui, X.; Zhang, W.; Yan, Q.; Chen, P.; Huo, F.; Huang, W.; Dong, X. MOF-directed templating synthesis of a porous multicomponent dodecahedron with hollow interiors for enhanced lithium-ion battery anodes. *J. Mater. Chem. A* **2015**, *3*, 8483–8488. [CrossRef]
234. Leng, W.; Cui, L.; Liu, Y.; Gong, Y. MOF-derived MnV₂O₄/C microparticles with graphene coating anchored on graphite sheets: Oxygen defect enganged high performance aqueous Zn-ion battery. *Adv. Mater. Interfaces* **2022**, *9*, 2101705. [CrossRef]
235. Zhang, X.; Zi, W.; Zhou, J.; Zhou, L.; Zhang, J.; Xuan, X. Li-Mn Bimetallic Metal-Organic Framework and Its Derivative as a Cathode for Lithium-Ion Batteries. *Inorg. Chem.* **2023**, *62*, 9501–9507. [CrossRef]
236. Li, H.; Dong, W.; Li, C.; Wang, Y.; Sun, M.-H.; Barakat, T.; Li, Y.; Su, B.-L. Boosting Reaction Kinetics and Shuttle Effect Suppression by Single Crystal MOF-Derived N-Doped Ordered Hierarchically Porous Carbon for High Performance Li-Se Battery. *Sci. China Mater.* **2022**, *65*, 2975–2988. [CrossRef]
237. Shen, C.; Li, Y.; Gong, M. Ultrathin Cobalt Phthalocyanine@Graphene Oxide Layer-Modified Separator for Stable Lithium–Sulfur Batteries. *ACS Appl. Mater. Interfaces* **2021**, *13*, 60046–60053. [CrossRef] [PubMed]
238. Wen, C.; Du, X.; Wu, F.; Wu, L.; Li, J.; Liu, G. Conductive Al-Doped Zno Framework Embedded With Catalytic Nanocages as a Multistage-Porous Sulfur Host in Lithium-Sulfur Batteries. *ACS Appl. Mater. Interfaces* **2021**, *13*, 44389–44400. [CrossRef] [PubMed]
239. Li, J.; Li, C.; Ren, J.; Zhang, K.; Wang, L. Synergistic Effect of Organic-Inorganic Hybrid Electrolyte for Ultra-Long Zn–I₂ Batteries. *Int. J. Hydrogen Energy* **2023**, *48*, 21985–21995. [CrossRef]
240. Ou, G.; Chen, J.; Lu, M.; Liu, J.; Zhang, X.; Lin, X.; Wu, Y.; Zeb, A.; Reddy, R.C.K.; Xu, Z. A Metal-Organic Framework Approach to Engineer ZnO/Co₃ZnC/N-doped Carbon Composite as Anode Material for Boosting Lithium Storage. *J. Alloys Compd.* **2022**, *923*, 166436. [CrossRef]
241. Hou, J.; Guo, Y.; Zhang, Y.; Li, J.; Xu, Y.; Fang, Z.; Yang, J.; Wu, M. Facile Green and Sustainable Synthesis of MnO@rGO as Electrochemically Stable Anode for Lithium-Ion Batteries. *Mater. Lett.* **2022**, *325*, 132761. [CrossRef]
242. Chu, K.; Li, Z.; Xu, S.; Yao, G.; Xu, Y.; Niu, P.; Zheng, F. MOF-Derived Hollow NiCo₂O₄ Nanowires as Stable Li-Ion Battery Anodes. *Dalton Trans.* **2020**, *49*, 10808–10815. [CrossRef]

243. Zhai, S.; Liu, W.; Hu, Y.; Chen, Z.; Xu, S.; Wu, L.; Ye, Z.; Wang, X.; Mei, T. Kinetic Acceleration of Lithium Polysulfide Conversion via a Copper-Iridium Alloying Catalytic Strategy in Li-S Batteries. *ACS Appl. Mater. Interfaces* **2022**, *14*, 50932–50946. [CrossRef]
244. Zhou, F.; Qiao, Z.; Zhang, Y.; Xu, W.; Zheng, H.; Xie, Q.; Luo, Q.; Wang, L.; Qu, B.; Peng, D.-L. Bimetallic MOF-Derived CNTs-Grafted Carbon Nanocages as Sulfur Host for High-Performance Lithium–Sulfur Batteries. *Electrochim. Acta* **2020**, *349*, 136378. [CrossRef]
245. Li, J.; Chen, L.; Wang, F.; Qin, Z.; Zhang, Y.; Zhang, N.; Liu, X.; Chen, G. Anionic Metal–Organic Framework Modified Separator Boosting Efficient Li-Ion Transport. *Chem. Eng. J.* **2023**, *451*, 138536. [CrossRef]
246. Zuo, L.; Ma, Q.; Xiao, P.; Guo, Q.; Xie, W.; Lu, D.; Yun, X.; Zheng, C.; Chen, Y. Upgrading the Separators Integrated with Desolvation and Selective Deposition Toward the Stable Lithium Metal Batteries. *Adv. Mater.* **2024**, *36*, 2311529. [CrossRef] [PubMed]
247. Yang, L.; Tian, Y.; Ge, P.; Zhao, G.; Pu, T.; Yang, Y.; Zou, G.; Hou, H.; Huang, L.; Ji, X. Perovskite ABO_3 -Type MOF-Derived Carbon Decorated Fe_3O_4 with Enhanced Lithium Storage Performance. *ChemElectroChem* **2018**, *5*, 3426–3436. [CrossRef]
248. Li, A.; Zhong, M.; Shuang, W.; Wang, C.; Liu, J.; Chang, Z.; Bu, X.-H. Facile synthesis of Co_3O_4 nanosheets from MOF nanoplates for high performance anodes of lithium-ion batteries. *Inorg. Chem. Front.* **2018**, *5*, 1602–1608. [CrossRef]
249. Zheng, F.; Zhu, D.; Shia, X.; Chen, Q. Metal–organic framework-derived porous $\text{Mn}_{1.8}\text{Fe}_{1.2}\text{O}_4$ nanocubes with an interconnected channel structure as high-performance anodes for lithium ion batteries. *J. Mater. Chem. A* **2015**, *3*, 2815–2824. [CrossRef]
250. Yan, Z.; Sun, Z.; Li, A.; Liu, H.; Guo, Z.; Zhao, L.; Feng, J.; Qian, L. Vacancy and architecture engineering of porous FeP nanorods for achieving superior Li^+ storage. *Chem. Eng. J.* **2022**, *429*, 132249. [CrossRef]
251. Cao, L.; Lv, F.; Liu, Y.; Wang, W.; Huo, Y.; Fu, X.; Sun, R.; Lu, Z. A high performance O₂ selective membrane based on CAU-L-NH₂@ polydopamine and the pmma polymer for Li–air batteries. *Chem. Commun.* **2015**, *51*, 4364–4367. [CrossRef]
252. Ding, J.; Du, T.; Thomsen, E.H.; Andresen, D.; Fischer, M.R.; Moller, A.K.; Petersen, A.R.; Pedersen, A.K.; Jensen, L.R.; Wang, S.; et al. Metal–organic framework glass as a functional filler enables enhanced performance of solid-state polymer electrolytes for lithium metal batteries. *Adv. Sci.* **2024**, *11*, e2306698. [CrossRef]
253. Chen, M.; Zhang, H.; Li, H.; Zhao, Z.; Wang, K.; Zhou, Y.; Zhao, X.; Dubal, D.P. CxNy-based materials as gas sensors: Structure, performance, mechanism and perspective. *Coord. Chem. Rev.* **2024**, *503*, 215653. [CrossRef]
254. Wang, G.; Hu, Y.; Yan, H.; Ren, X.; Yang, L.; Huang, Z.; Wu, X. Effects of F substitution on crystal structure, band characteristics and microwave dielectric properties of $\text{Li}_3\text{Mg}_2\text{NbO}_6$ ceramics for high frequency applications. *Ceram. Int.* **2024**, *50*, 17097–17105. [CrossRef]
255. Cheng, X.; Pan, Q.; Tan, H.; Chen, K.; Liu, W.; Shi, Y.; Dua, S.; Zhu, B. The construction of an efficient magnesium–lithium separation thin film composite membrane with dual aqueous-phase monomers (PIP and MPD). *RSC Adv.* **2023**, *13*, 22113–22121. [CrossRef]
256. Wu, W.; Xia, R.; Qian, G.; Liu, Z.; Razavi, N.; Berto, F.; Gao, H. Mechanostructures: Rational mechanical design, fabrication, performance evaluation, and industrial application of advanced structures. *Prog. Mater. Sci.* **2023**, *131*, 101021. [CrossRef]
257. Saapi, S.S.Y.; Andrianisa, H.A.; Zorom, M.; Mounirou, L.A.; Kouassi, H.A.A.; Ahossouhe, M.S. New developments on vermicfiltration as a bio-ecological wastewater treatment technology: Mechanism, application, performance, modelling, optimization, and sustainability. *Heliyon* **2024**, *10*, e25795. [CrossRef] [PubMed]
258. Andersson, M.; Yuan, J.; Sundén, B. Review on modeling development for multiscale chemical reactions coupled transport phenomena in solid oxide fuel cells. *Appl. Energy* **2010**, *87*, 1461–1476. [CrossRef]
259. Hu, J.; Zhu, Y.; Huang, H.; Lu, J. Recent advances in shape–memory polymers: Structure, mechanism, functionality, modeling and applications. *Prog. Polym. Sci.* **2012**, *37*, 1720–1763. [CrossRef]
260. Le, T.; Epa, V.C.; Burden, F.R.; Winkler, D.A. Quantitative Structure Property Relationship Modeling of Diverse Materials Properties. *Chem. Rev.* **2012**, *112*, 2889–2919. [CrossRef]
261. Ji, C.; Dai, J.; Zhai, C.; Wang, J.; Tian, Y.; Sun, W. A Review on Lithium-Ion Battery Modeling from Mechanism-Based and Data-Driven Perspectives. *Processes* **2024**, *12*, 1871. [CrossRef]

Disclaimer/Publisher’s Note: The statements, opinions and data contained in all publications are solely those of the individual author(s) and contributor(s) and not of MDPI and/or the editor(s). MDPI and/or the editor(s) disclaim responsibility for any injury to people or property resulting from any ideas, methods, instructions or products referred to in the content.